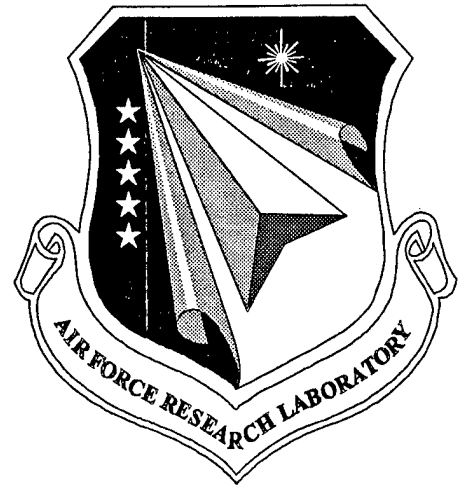


**AFRL-ML-WP-TR-1999-4144**

**FILMLESS RADIOGRAPHY FOR  
AEROSPACE APPLICATIONS**



**PETER SOLTANI  
MICHAEL NEARY**

**LIBERTY TECHNOLOGIES  
A DIVISION OF CRANE NUCLEAR, INC.  
555 NORTH LANE  
CONSHOHOCKEN, PA 19428-2208**

**JULY 1999**

**FINAL REPORT FOR JAN 1997 – JUL 1999**

**APPROVED FOR PUBLIC RELEASE; DISTRIBUTION UNLIMITED**

**20000406 102**

**MATERIALS AND MANUFACTURING DIRECTORATE  
AIR FORCE RESEARCH LABORATORY  
AIR FORCE MATERIEL COMMAND  
WRIGHT-PATTERSON AIR FORCE BASE OH 45433-7750**


**DTIC QUALITY INSPECTED 1**


## NOTICE


WHEN GOVERNMENT DRAWINGS, SPECIFICATIONS, OR OTHER DATA ARE USED FOR ANY PURPOSE OTHER THAN IN CONNECTION WITH A DEFINITELY GOVERNMENT-RELATED PROCUREMENT, THE UNITED STATES GOVERNMENT INCURS NO RESPONSIBILITY OR ANY OBLIGATION WHATSOEVER. THE FACT THAT THE GOVERNMENT MAY HAVE FORMULATED OR IN ANY WAY SUPPLIED THE SAID DRAWINGS, SPECIFICATIONS, OR OTHER DATA, IS NOT TO BE REGARDED BY IMPLICATION OR OTHERWISE IN ANY MANNER CONSTRUED, AS LICENSING THE HOLDER OR ANY OTHER PERSON OR CORPORATION, OR AS CONVEYING ANY RIGHTS OR PERMISSION TO MANUFACTURE, USE, OR SELL ANY PATENTED INVENTION THAT MAY IN ANY WAY BE RELATED THERETO.

THIS REPORT IS RELEASABLE TO THE NATIONAL TECHNICAL INFORMATION SERVICE (NTIS). AT NTIS, IT WILL BE AVAILABLE TO THE GENERAL PUBLIC, INCLUDING FOREIGN NATIONS.

THIS TECHNICAL REPORT HAS BEEN REVIEWED AND IS APPROVED FOR PUBLICATION.

  
BRYAN SANBONGI, Project Engineer  
Nondestructive Evaluations Branch  
Metals, Ceramics & NDE Division

  
JAMES C. MALAS, Chief  
Nondestructive Evaluations Branch  
Metals, Ceramics & NDE Division

  
GERALD J. PETRAK, Assistant Chief  
Metals, Ceramics & NDE Division  
Materials & Manufacturing Directorate

IF YOUR ADDRESS HAS CHANGED, IF YOU WISH TO BE REMOVED FROM OUR MAILING LIST, OR IF THE ADDRESSEE IS NO LONGER EMPLOYED BY YOUR ORGANIZATION, PLEASE NOTIFY, AFRL/MLLP, WRIGHT-PATTERSON AFB OH 45433-7817 AT (937) 255-9819 TO HELP US MAINTAIN A CURRENT MAILING LIST.

COPIES OF THIS REPORT SHOULD NOT BE RETURNED UNLESS RETURN IS REQUIRED BY SECURITY CONSIDERATIONS, CONTRACTUAL OBLIGATIONS, OR NOTICE ON A SPECIFIC DOCUMENT.

REPORT DOCUMENTATION PAGE			Form Approved OMB No. 0704-0188	
Public reporting burden for this collection of information is estimated to average 1 hour per response, including the time for reviewing instructions, searching existing data sources, gathering and maintaining the data needed, and completing and reviewing the collection of information. Send comments regarding this burden estimate or any other aspect of this collection of information, including suggestions for reducing this burden, to Washington Headquarters Services, Directorate for Information Operations and Reports, 1215 Jefferson Davis Highway, Suite 1204, Arlington, VA 22202-4302, and to the Office of Management and Budget, Paperwork Reduction Project (0704-0188), Washington, DC 20503.				
1. AGENCY USE ONLY (Leave blank)		2. REPORT DATE JULY 1999		3. REPORT TYPE AND DATES COVERED FINAL REPORT FOR JAN 1997 - JUL 1999
4. TITLE AND SUBTITLE FILMLESS RADIOGRAPHY FOR AEROSPACE APPLICATIONS			5. FUNDING NUMBERS C F33615-97-C-5122 PE 78011 PR 2865 TA 02 WU 07	
6. AUTHOR(S) PETER SOLTANI MICHAEL NEARY				
7. PERFORMING ORGANIZATION NAME(S) AND ADDRESS(ES) LIBERTY TECHNOLOGIES A DIVISION OF CRANE NUCLEAR, INC. 555 NORTH LAKE CONSHOHOCKEN, PA 19428-2208			8. PERFORMING ORGANIZATION REPORT NUMBER	
9. SPONSORING/MONITORING AGENCY NAME(S) AND ADDRESS(ES) MATERIALS AND MANUFACTURING DIRECTORATE AIR FORCE RESEARCH LABORATORY AIR FORCE MATERIEL COMMAND WRIGHT-PATTERSON AFB, OH 45433-7750 POC: BRYAN SANBONGI, AFRL/MLLP, 937-255-9801			10. SPONSORING/MONITORING AGENCY REPORT NUMBER  AFRL-ML-WP-TR-1999-4144	
11. SUPPLEMENTARY NOTES				
12a. DISTRIBUTION AVAILABILITY STATEMENT  APPROVED FOR PUBLIC RELEASE, DISTRIBUTION UNLIMITED.			12b. DISTRIBUTION CODE	
13. ABSTRACT (Maximum 200 words) The aim of this effort was to develop, deliver, and implement three systems for acquiring digital radiographic images of the requisite quality to meet Air Force aircraft inspection requirements. The systems employ storage phosphor technology and help to eliminate the chemical waste and delays with conventional radiography employing film. This effort has succeeded in developing improved large area storage phosphor imaging systems capable of achieving the requisite 2%-2T image quality requirement over a range of applications useful for aircraft inspections. Moreover, system performance and reliability have been evaluated, indicating that the system is suitable for use in the field,				
14. SUBJECT TERMS Storage of Phosphor technology, filmless radiography, corrosion			15. NUMBER OF PAGES 67	
			16. PRICE CODE	
17. SECURITY CLASSIFICATION OF REPORT UNCLASSIFIED	18. SECURITY CLASSIFICATION OF THIS PAGE UNCLASSIFIED	19. SECURITY CLASSIFICATION OF ABSTRACT UNCLASSIFIED	20. LIMITATION OF ABSTRACT SAR	

## TABLE OF CONTENTS

<b>Section</b>	<b>Page</b>
<b>1.0 SUMMARY</b>	<b>1</b>
<b>2.0 INTRODUCTION</b>	<b>5</b>
<b>3.0 BACKGROUND</b>	<b>8</b>
3.1 General System Description	8
3.2 Storage Phosphor Description	9
3.3 Readout and Digitization	13
3.4 Display Architecture	15
<b>4.0 IMAGE QUALITY IMPROVEMENTS</b>	<b>18</b>
4.1 Storage Phosphor Optimization	18
4.2 Scanner Improvements	24
4.3 Image Processing	29
<b>5.0 14" SCREENS</b>	<b>38</b>
5.1 Scale-up of Screen Fabrication Process	38
5.2 Reusability Testing	
(Subcontract to Southwest Research Institute)	40
<b>6.0 DEVELOPMENT OF 14" CASSETTES</b>	<b>45</b>
<b>7.0 ERASER DEVELOPMENT</b>	<b>45</b>
7.1 Erase process optimization	45
7.2 Sheet metal Design	46
<b>8.0 APPLICATIONS RESULTS</b>	<b>48</b>
<b>9.0 CONCLUSIONS</b>	<b>50</b>
<b>10.0 RECOMMENDATIONS</b>	<b>53</b>
<b>11.0 REFERENCES</b>	<b>54</b>
APPENDIX I	55
APPENDIX II	59

## LIST OF FIGURES

Figure		Page
1.	Filmless radiography program summary.	1
2.	Input-output characteristics of SrS:Ce, Sm storage phosphor	10
3.	Trap filling rate for SrS:Ce,Sm.	11
4.	Storage phosphor screen cross-section.	13
5.	Logistic (solid) overlaid on window/level characteristic curve (dotted).	30
6.	An original image and its histogram before (left) and after (right) histogram equalization.	31
7.	Step function before and after low pass filtering (top), and before and after unsharp mask processing (bottom).	33
8.	Turbine blade (a) before and (b) after statistical differencing.	35
9.	Example of Kirsch filter.	36
10.	2% ASTM penetrameters on aluminum step wedge.	46
11.	Lead resolution pattern exposed and scanned at 70 microns, showing 7 Lp/mm resolution.	46
12.	Full 14"x17" image of composite phantom of object, aluminum blocks, and line pair gauge.	47
13.	X-ray image of Ni orbital tune weld, approximately 19 mm in diameter.	47

## LIST OF TABLES

Tables		Page
1.	Typical phosphor imaging applications.	4
2.	Phosphor screen test summary.	18

## **FOREWORD**

This report describes the work performed under U.S. Air Force contract F33615-97-C-5122, "Filmless Radiography," from January 1997 through July 1999. The Air Force NDI Program Office initially conducted a Phase I SBIR with Liberty Technologies to determine if filmless radiography is technically feasible and economically viable for the inspection of Air Force weapon systems in both the depot and field environments. In particular, the program looked at inspection of F-15 and T-38 aircraft for FOD, moisture, corrosion, and cracks as well as the system's mobility. The mobility of this PC-based system was also demonstrated by frequently moving it from one location to another. Air Force Research Laboratory (then Wright Laboratory)'s Manufacturing Technology Directorate, in cooperation with the NDE Branch and NDI Program Office, and supported by the Aging Aircraft Program, then funded the program to enhance the RADView filmless radiography system's sensitivity and enlarge the image format.

The technical effort was conducted by Liberty Technologies, A Division of Crane Nuclear, Inc. under the direction of Project Managers: Ms. Diana Carlin, AFRL/MLMP and Mr. Charles Buynak, AFRL/MLLP.

This report was compiled and written by Mr. Peter Soltani and Michael Neary of Liberty Technologies.

## 1. SUMMARY

The United States Air Force has undertaken a program to evaluate, develop, and implement an effective, affordable, mobile system of filmless radiography. While radiography is a widely used NDI technique, there have been very few major technological advances in the last 100 years. Storage phosphor technology provides the potential of utilizing all the advantages of digital imaging as well as eliminating the HAZMAT issues related to film processing.

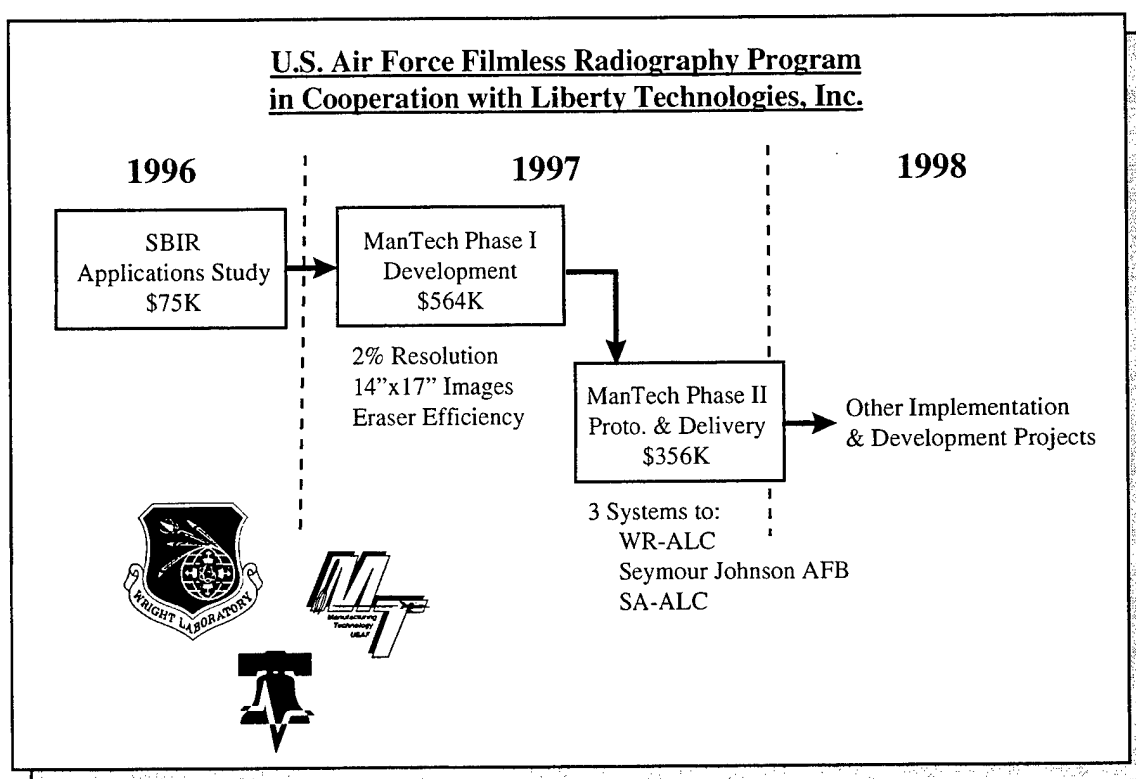


Figure 1. Air Force radiography program summary.

The Air Force NDI Program Office initially conducted a Phase I SBIR project with Liberty Technologies to determine if filmless radiography is technically feasible and economically viable for the inspection of Air Force weapon systems in both the depot and field environments. In particular, the program looked at inspection of F-15 and T-38 aircraft for FOD, moisture, corrosion, and cracks as well as the system's mobility.



Liberty's RADView filmless radiography system was evaluated at Kelly AFB, Randolph AFB, Robins AFB, and Tyndal AFB, and confirmed the system's ability to acceptably detect foreign objects, moisture, corrosion, and some cracks. The mobility of this PC-based system was also demonstrated by frequently moving it from one location to another. Wright Laboratory's Manufacturing Technology Directorate, in cooperation with the NDE Branch and the NDI Program Office, and supported by the Aging Aircraft Program, then funded a program to enhance RADView's sensitivity and enlarge the image format. RADView is now capable of producing 2% object contrast sensitivity and images from 3"x5" to 14"x17" and any size in between, both being key program requirements.

The first three prototypes of this system were installed at the 4th Fighter Wing at Seymour Johnson AFB, WR-ALC at Robins AFB, and at SA-ALC at Kelly AFB; these have since been moved to Edwards AFB, Tinker AFB, and the third remains at Robins AFB. A fourth Air Force system is available through Liberty for demonstration or applications analysis at other locations.

Demonstration of 2% sensitivity on aluminum was a requirement of the program. However, as an additional indication of the new performance of the system, a comparison was made of film and phosphor inspections of one of the U.S. Navy's certification standards. This standard was a piece of aluminum structure from an F/A-18 that contained actual fatigue cracks. Phosphor showed several cracks that film missed and film showed several cracks that phosphor missed. This is exactly what one would have predicted for comparable performance.

The current phosphor system has successfully been used to good effect with x-ray energies from 18 kV to 200 kV, as well as Ir-192 gamma radiography. Some of the materials and configurations that have been examined with a sensitivity of 2-2T include wrought and cast aluminum, titanium, and steel from 1/8" to 1" in thickness. Specific applications that have been successful are shown in Table 1 and include the examination

of wax casting patterns, and turbine blades, some of which contain very small cooling passages. These passages are inspected for small inclusions of foreign material.

While there is an extremely wide range of composite materials and configurations, we have successfully looked at quite a few (enough to give considerable confidence in the ability to look at others). Aluminum, fiberglass, and paper bonded honeycomb panels were examined for excess or missing adhesive, crushed core, and mislocated components. More complex applications have included mixed combinations of materials such as graphite, fiberglass, and aluminum. Depending on the particular materials, it is also possible to interpret fiber orientation and proper lay up.

Erosion/corrosion evaluation has also been performed on a variety of pipes, especially steel up to 6 inch diameter with external insulation installed. These included wall thickness reduction due to erosion as well as the buildup of microorganisms. Ordinance (bombs), especially because of the wide latitude involved, are a particularly good application now that the system has been improved. Generally, this involves looking through a thick steel case to evaluate what it is filled with (e.g., high explosive or chemical agent, how full it is, etc.) or even more importantly to evaluate the fuse. It is extremely important to determine the type and condition of these electromechanical devices prior to any attempts to dispose of them.

As part of the Air Force development effort, Southwest Research Institute performed an analysis of the reusability of the phosphor screens. A Liberty phosphor screen was subjected to 520 exposure/scanning/erasure cycles. The concept was to x-ray a test phantom, read and store the image, erase the image, and then do the same test over and over to the same screen. Based on the data that was obtained, no trend of image degradation was observed.

**Table 1. Typical Phosphor Imaging**

<u>Configuration</u>	<u>Material</u>	<u>Condition</u>
Plate and castings, 1/8" - 1"	Aluminum, Titanium, Steel	Weld and casting defects
Tube / Pipe, 1" to 6" dia.	Aluminum, Steel	Weld defects, wall thinning from erosion/corrosion, micro-organism buildup.
Composites (honeycomb)	Aluminum, Fiberglass	Crushed core, entrapped moisture, missing or excess adhesive, misaligned structural elements. corrosion
Composite laminates	Graphite and Fiberglass, Tape and Fabric, Various Processes	Adhesive uniformity, improper layup or fiber orientation,
Aircraft structure (skins, spars, frames, systems)	Aluminum, Titanium	Cracks, Corrosion, FO, presence or condition of seals, fluid levels, etc.
Turbine Blades	Titanium, Hi Temp Steels	Casting defects and foreign material
Printed Circuit Boards	Silicon, Fiberglass, Copper, Aluminum, etc.	Component placement and connections, uniformity of potting compounds
Ordinance (Explosives)	Steel, Aluminum, Copper, Organics	Type and condition of fuze and explosive

Economic analysis reveals cost savings that would yield a potential return on investment of approximately one year for an F-15 wing of 70+ aircraft, based on film costs alone (see Appendix I). Other potential cost savings include paperwork reduction and weight savings resulting from not having to take film processing chemicals and equipment on deployment; and being able to perform the entire inspection in the phase dock or other location rather than in the NDI lab, and elimination of the dark room.

## 2.0 INTRODUCTION

The objective of this program was to provide, at low risk and in the near term, a practical and reliable system of digital radiography to the Air Force that will provide immediate economic and environmental benefits. Liberty Technologies had previously shown the feasibility of employing storage phosphor technology to replace film for low resolution x-ray radiography tasks routinely performed by the Air Force during aircraft inspection and maintenance. This system employs a 7" wide storage phosphor screen which captures and retains an x-ray image; this latent image can then be read by a laser scanning device to remove and digitize the image for viewing on a computer workstation, thereby eliminating the need for chemical and waste by products. However, the previous system did not have the requisite image quality and image capture field of view needed to justify broad based conventional film replacement. The aim of the present project has been to build on the previous experience with the lower resolution and smaller field of view storage phosphor system independently developed by Liberty and to develop a new system with the required field of view and image quality.

The specific objectives of the program are as follows:

1. Develop a storage phosphor readout device capable of scanning screens from 2" to 14" wide, and lengths up to 17".
2. Produce flexible screens and cassettes from 2" to 14" wide and up to 17" long.
3. Achieve an overall performance capability of 2% contrast sensitivity with digital scan resolution of 50  $\mu$ m pixels up to a 10" width and 70 $\mu$ m pixels over a 10" width.
4. Increase phosphor screen latent image removal throughput.

5. Manufacture, deliver, and implement three filmless radiography systems at select Air Force sites.

In meeting the objectives of this program Liberty pursued four major technical areas in parallel. They were:

#### Image Quality Improvement

1. Improving the resolution and efficiency of the phosphor screens.
2. Improving the resolution and signal-to-noise ratio of the laser readout system.
3. Investigating image processing techniques to aid in defect detection.

#### Manufacturing Scale-up

1. Developing 14" wide readout system, which included design of the necessary optics, a larger transport system, and a longer light collector.
2. Scale up storage phosphor screen manufacturing process to produce 14" wide media with high yield and quality.
3. Re-design phosphor screen eraser (this is to remove any residual latent image prior to screen re-use) to improve erase time.
4. Design large cassettes to accommodate larger screens.
5. Modify existing applications software to interface and acquire images from new scanner, as well as providing digital image display, analysis, and archiving to handle substantially larger image file sizes generated with the new system.

## 6. Performance evaluation and reliability.

Before reviewing the specific tasks and the results of the efforts, it is worth reviewing in general terms the technical basis for the storage phosphor technology. The summary below should help put the overall aims of the effort and the challenges encountered in a clear technical perspective.

### 3.0 BACKGROUND

Industrial radiographic imaging remains one of the best methods to visually inspect, diagnose, and measure the integrity of manufactured products. Though advances have been made in real-time digital radiography methods, the vast majority of radiography is still performed with conventional radiographic film, a method dating back to the discovery of x-rays 100 years ago. The reasons for the limited replacement of film by conventional digital radiography methods include the expense and generally large size of available systems. Though real-time systems can be cost effective for inspections in a high volume manufacturing environment, they cannot compete with the relatively low expense of film in most radiography, and in particular, field radiography applications.

In order to help overcome the barriers to film and real-time radiography approaches, a unique filmless inspection system based on *storage phosphor* sensor technology has been developed. With this method, radiography can be performed in a fashion very similar to conventional film, but with a dry optical readout process and a digital result.

#### 3.1 General System Description

The filmless radiography system developed under this program employs a storage phosphor material deposited on a flexible substrate which when exposed to radiation, absorbs and stores the radiation energy in the form of trapped electrons. The trapped electron population density is correlated both spatially and in amplitude to the input radiation intensity pattern, and thus called a *latent image*. The trapped electron population is metastable and can remain in the state for extended time periods (e.g., days), though gradual recombination of trapped electrons occurs resulting in loss of stored energy. However, the recombination can be accelerated by selective optical stimulation, resulting in the emission of characteristic visible luminescence. Again, since the luminescence is correlated to the latent image, it has the character of the original radiation image. In this way, the storage phosphor acts as an energy transducer, converting the radiation pattern to

a visible light pattern. Since the processes are completely reversible, the sensor can undergo a vast number of cycles without noticeable degradation.

The readout and digitization of the storage phosphor takes place by scanning the sensor with a laser whose focal spot size determines the system resolution limit. The emitted luminescence from each element is captured and propagated to a photomultiplier tube (PMT), where it is converted to an electrical signal. The analog signal is amplified, digitized and stored in computer memory as a function of laser position on the sensor. When the entire sensor has been scanned, the final image is computed and displayed on a CRT - this process is sometimes referred to as *computed radiography (CR)*.

Once a digital radiographic image of an object is created, then a wide range of analysis and processing functions can be employed. These range from simple dimensional measurements to more complex flaw detection and sizing algorithms.

### **3.2 Storage Phosphor Description**

#### *Input/Output Characteristics*

The storage phosphor sensor employed in this system is a strontium sulfide (SrS) host crystal doped with trace amounts of rare-earth elements cerium (Ce) and samarium (Sm). SrS has the general crystalline structure of sodium chloride (face-centered cubic sublattice), and is considered a wide band-gap semiconductor with an indirect gap energy of approximately 4 eV. When the rare-earth ions are introduced to the lattice, they occupy substitutional positions within the lattice. A general diagram representing the sensor characteristics is shown in Figure 2.



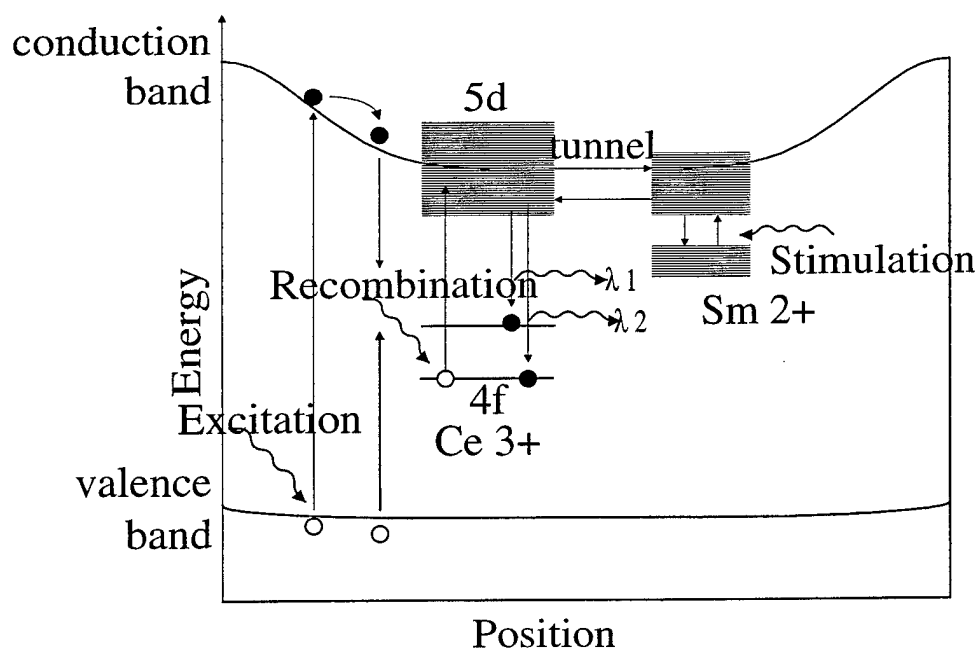


Figure 2. Input-output characteristics of SrS:Ce, Sm storage phosphor

The steps taking place in Figure 2 are as follows:

1. Incident ionizing radiation is absorbed by the host crystal, generating electron-hole pairs (excitation).
2. Electron-hole pairs lose energy and preferentially recombine at  $\text{Ce}^{3+}$  sites.
3. Recombination energy is transferred to the 4f electron of the  $\text{Ce}^{3+}$ .
4. 4f electron is excited to the 5d energy state.
5. 5d electron can transition back to the 4f state and radiate energy (fluoresce) or tunnel to the  $\text{Sm}^{3+}$ , becoming trapped and converting the  $\text{Sm}^{3+}$  to  $\text{Sm}^{2+}$ .

6. The electron trapped at the  $\text{Sm}^{2+}$  can be stimulated with 1 micron wavelength near-infrared (IR) energy and tunnel back to the Ce ion.
7. The stimulated electron transitions from the 5d state to the 4f ground states, radiating energy (photostimulated luminescence, *PSL*) and returning to its original state.

It can be seen that steps 1-5 involve the conversion of the radiation energy to proportional population of trapped electrons. Within a 2-dimensional sensor, these steps are associated with creating a latent radiographic image. The buildup of trapped electrons can be summarized by the following expression:

$$n(t) = N[1 - \exp(-ft/N)]$$

where,  $N$  is the maximum available number of trapping sites,  $f$  is the excitation rate, and  $t$  is the exposure time. Note that  $ft = \gamma D$ , where  $D$  is the radiation dose and  $\gamma$  is a proportionality factor. It is shown in Figure 3 that when  $n$  is plotted against exposure time (or radiation dose), the number of trapped electrons increase linearly until saturation.

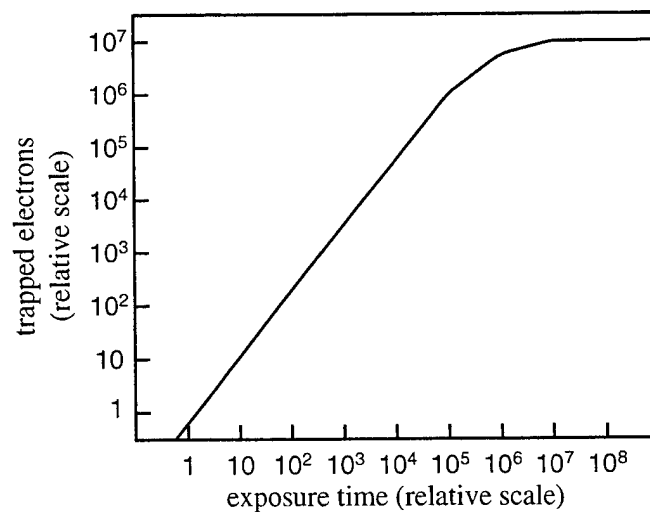


Figure 3. Trap filling rate for SrS:Ce,Sm.

Steps 6 & 7 correspond to the readout of the latent image by optical stimulation. The lump-sum rate at which the trapped electrons are photostimulated and eventually relax to produce luminescence can be given by,

$$dn/dt = -\sigma I$$

where,  $\sigma$  is the photon capture efficiency by the  $\text{Sm}^{2+}$  ions, and  $I$  is the intensity absorbed by the storage phosphor. It can be noted that  $\sigma I$  has units of inverse time, thus representing the time constant for the trap emptying process. It is also noted that the rate at which luminescence (the instantaneous PSL intensity) is produced is directly proportional to the IR intensity. Finally, the time integral of the process is constant, meaning the total amount of luminescence which can be produced for a given initial population of trapped electrons is constant.

Once the electrons have been completely returned to their original state, the entire process can be repeated. It is important to note that the population of trapped electrons and the PSL intensity are linearly related to the incident ionizing radiation energy. It is further noted that the population of trapping sites is large, resulting in greater exposure latitude (dynamic range) than conventional radiographic film or even semiconductor detectors.

### *Sensor Structure*

Figure 4 shows the typical structure of the storage phosphor sensor. Since the exposure and readout properties are optical and do not require electrical contact to the sensor, it can be fabricated in the form of a thin granular layer adhered to a flexible plastic substrate. An optically clear overcoat is applied to provide mechanical durability. The properties of the sensor, such as spatial resolution, contrast, and quantum efficiency, are related to the structure. These properties are similar to conventional film. For example, a fine grain sensor will exhibit high spatial resolution whereas a coarse grain screen will show lower

resolution but higher quantum efficiency. In general, the properties of the sensor can be tailored for different types of radiographic imaging applications.

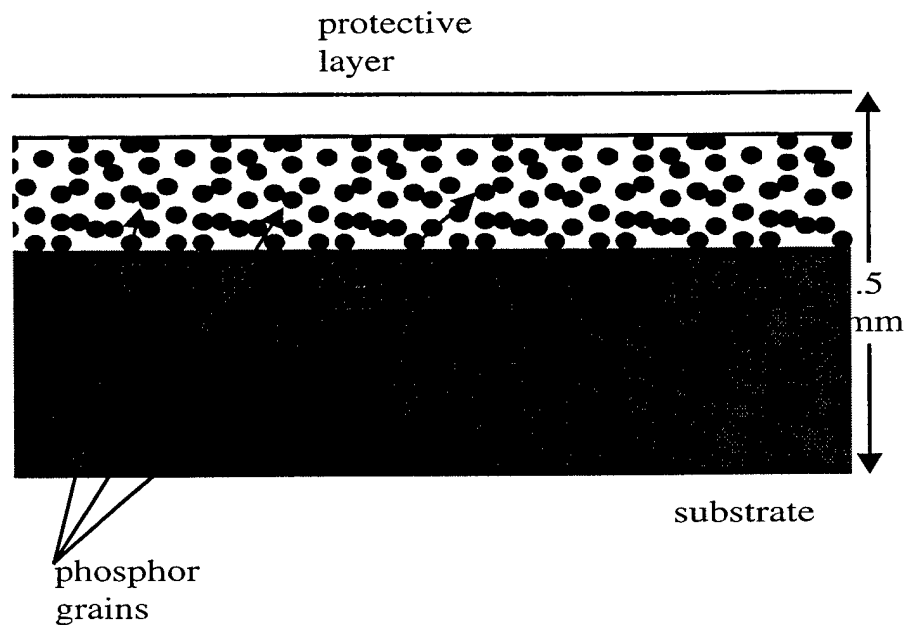


Figure 4. Storage phosphor screen cross-section.

### 3.3 Readout and Digitization

#### *Readout*

Readout of the information stored in a storage phosphor sensor is best accomplished by scanning it with an infrared laser beam. In the present system, a 50 micrometer diameter (FWHM) laser is employed to scan the sensor. While the near-IR is scanned across the sensor at a constant velocity, PSL is generated along this line. Since each scan is along a stationary line, the sensor is also indexed at a constant velocity normal to the scan line to achieve 2-dimensional readout. The scan and index velocities are accurately synchronized to maintain pixel errors less than 25% of the pixel size and a uniform aspect ratio of unity.

Since a flying-spot is employed, the size of each pixel is the product of laser scan velocity (approximately 1,000 cm/second) and the sampling period (5 microseconds). By varying the sampling period, the pixel pitch of the system can be varied from 50 microns to any larger value. Under optimum exposure conditions, a 50 micron limiting resolution can be achieved with the system.

### *Digitization*

In order to generate a digital radiograph, the PSL is collected by a light collector and propagated to a PMT. A unique feature of the RADView system is that a log-amplifier is employed to convert the linear PMT output to log-space. Since the aim of radiographic inspection is to image small changes in object density, simply digitizing the linear output of the PMT would result in uneven sampling of contrast changes. What is important is to uniformly digitize *relative* changes in contrast. With linear digitization, a signal change of 1-10 is represented by 9 digital units and has equal weight as a signal change of 11-20. However, an object contrast change of 1-10 (an order of magnitude!) is not equal to a change of 9 but rather a ten-fold change. By employing a log-amplifier, the digitized values equally represent relative changes in contrast.

The analog signal is digitized with a 12 bit analog-to-digital converter (ADC) and stored in computer memory as a function of laser position. Once the entire sensor has been scanned and all points digitized, the computed PSL intensities are converted to gray scale values and displayed on a CRT.

### *Performance characteristics*

The properties of a radiographic imaging system which define performance include exposure response, dynamic range (latitude), contrast sensitivity and spatial resolution. Storage phosphor systems are capable of capturing a significantly wider range of information than conventional film. However, it can also be seen that film exhibits a

steep response slope, meaning that a small change in exposure produces a large change in film density. Though phosphor exhibits a linear response, once the data has been digitized, it is possible to vary the slope digitally to selectively display a narrow range of exposure over the available range of gray scale values. In this way, a given contrast sensitivity can be achieved over a much wider range of object densities than with conventional film.

Contrast sensitivity measures the system's ability to detect very small changes in object density due to anomalies such as cracks, voids, or dimensional changes from in-service wear. Typically, engineering codes require that 2% contrast sensitivity must be achieved in radiographic imaging. The system described here meets this condition under optimum geometric exposure conditions over a wide range of exposure energies.

The resolution of an imaging system is generally defined in terms of the contrast difference detected between two closely spaced features. Analogous to a time varying signal, the contrast is equivalent to the signal amplitude and the object spacing (or period) is more conveniently specified in terms of spatial frequency (cycles per unit length). As previously indicated, the readout system achieves a 50 micron, or 10 Lp/mm scan resolution. Under optimum exposure conditions, a total image resolution of 10 Lp/mm has been achieved.

### **3.4 Display Architecture**

#### *General hardware layout*

Though a wide variety of computing platforms are available for display workstation, Liberty chose to employ PC-based hardware for cost, availability, and maintenance ease for the end-users. The system consists of networked archival and display CPU's. The archival CPU is configured with an SVGA display for data entry and viewing, including 8 bit images. In addition, the archival CPU is the gateway to peripheral devices, including a

variety of mass storage options, printers, and digitizers (phosphor, radiographic film, and documents). The display CPU employs a pentium processor with a minimum of 128 Mb of RAM for 12 bit image data processing and display mapping. Gray scale monitors with display resolutions up to 5 Mpixel are available; these high resolution gray scale monitors are driven by dedicated video boards.

### *Software architecture*

The software configuration matches the hardware layout. An archive software tool is provided for record management. The software has been designed to match work-flow logic and to provide user definable fields to track a vast array of NDT related information. These include radiographic exposure parameters, inspection parameters, object information, facility information, etc. The archival software is also structured with multi-level folders so that multiple images can be maintained in a single location. A variety of attachments can also be made to the primary image record, such as scanned documents or photographs, other NDT data or reports, etc.

The display software tool provides image analysis and processing to enhance the reproducibility of interpretations. Analysis functions include line profile of image density to measure object dimensions (such as pipe wall thickness loss over time); a magnification correction is also provided to speed dimensional measurements. The display processing includes gray scale mapping, as well as various thresholding functions to precisely select specific density regions for display.

The system offers several fixed sharpening and smoothing kernels, as well as the ability to generate custom kernels up to 9x9. Zoom and pan/scroll functions are also provided; these can be applied to the entire image or a selected region. In this way, a magnifying glass can be created to precisely investigate image regions while maintaining the full image in view. All processing or analysis function key-strokes can be saved with a macro recorder and played back to reproduce all viewing and interpretation conditions. Regions

can be annotated with normal text and arrows to identify indications, as with conventional film.

### *Gray scale mapping*

Display of radiographic images must be done carefully to ensure that proper interpretations can be made. This means that the system must properly map the 12 bit digital gray scale data to a CRT. First, since only 8 bits can be displayed on the monitor, a dynamic LUT function is provided so that the user can select which 256 gray scale range of the original 12 bit data is displayed; this is referred to as window and leveling. If all 12 bits are mapped, the LUT equally divides the 4096 gray levels over the available 256 display levels. Typically, useful radiographic information is contained over a narrow range of gray levels so that a window brackets the desired values within the 12 bit range to map to the display and the level of the window modulates the display brightness. In this way, it is possible to maximize the display contrast associated with small changes in object contrast.

### *Pixel mapping*

Another critical aspect of the electronic display is the resolution. Typically, CRT's with display resolutions of 1200x1600 or 2000x2500 are employed. However, scan resolutions up to 5000x6000 can be generated from the readout process. The system allows the user to employ either pixel replication or pixel interpolation when magnifying beyond the image resolution.



## **4.0 IMAGE QUALITY IMPROVEMENTS**

### **4.1 Storage Phosphor Optimization**

A measurement study aimed at observing the effect that varying storage phosphor metallurgical and fabricated screen parameters has on the imaging performance of the system was performed. Phosphor variations included metallurgical composition, heat treating, and particle size. Screen parameters included phosphor powder loading in the binder material, layer thickness, and overcoat process. The screens were fabricated with a range of variations and tested to determine the influence of the changes on resolution, efficiency, which together determine contrast sensitivity.

#### **4.1.1 Method**

Test data was acquired employing the x-ray facility at PCT, Inc., York, PA. The exposure setup included a Nuclear Associates resolution bar pattern, an Aluminum step wedge (up to 1.0"), and 0.5" and 0.25" Al blocks with 2%, 3%, and 4% penetrameters. Exposures at 60kV for 60mAs and 125mAs were completed for this report. Two 7" format scanners were employed for the screen readout. These systems exhibit only a 100 micron laser resolution and lack the improvements implemented in the 14" scanners developed under this program, but for the purposes of screen parameter comparisons, they were adequate.

Eighteen phosphor screens were tested. The makeup of each screen is shown in Table 2. To analyze the effect of each phosphor parameter on imaging performance, three measurements are taken on each image: Square Wave Response (SWR), Wiener noise spectra, and Signal-to-Noise Ratio (SNR). The SWR is measured by taking a minimum of 100 horizontal data lines taken transversely across a Nuclear Associates bar pattern from 2.0 to 5.0 line pairs per mm. The results from each line are averaged and normalized to the signal output difference at 0.05 line pairs per mm.

Table 2. Phosphor screen binder and thickness matrix

Screen number	Phosphor	Binder type	Binder %	Thickness (mil)	Coating
2060	Standard	Standard	4.5	4.5	Scrn Print
2061	Standard	Standard	4.5	4.5	Scrn Print
2204-02	Standard	Standard	10	4.5	Scrn Print
2204-04	Standard	Standard	12	4.5	Scrn Print
2204-06	Standard	Standard	15	4.5	Scrn Print
9701-42	No Barium	Standard	4.5	4.5	Nylon
2204-03	Standard	Standard	10	4.5	Nylon
2219-02	Standard	Standard	9	4.5	Scrn Print
R&D101	Standard	Standard	4.5	1	Scrn Print
R&D103	No Barium	B250	6.25	4.5	Scrn Print
R&D105	Standard	B250	12.5	4.5	Scrn Print
SMI	Standard	B250	12.5	3.5	Scrn Print
97042425	Standard	Standard	6	4.5	Scrn Print
97671001	Standard	B250	12.5	3.5	Nylon
2160-06	Standard	Standard	4.5	6	Scrn Print
2159-05	Standard	Standard	4.5	8	Scrn Print
2187-07	Standard	Standard	4.5	10	Scrn Print
2173-10	Standard	Standard	4.5	13	Scrn Print

The Wiener noise spectra is basically an FFT of horizontal lines measured across a minimum 200x512 pixel area of bare phosphor. The resulting spectra are averaged and displayed in the range between 0 and 5 line pairs per millimeter.

The SNR is the ratio of the difference in the mean phosphor densities of the 1/8" and 3/8" steps divided by the arithmetic mean of each step's standard deviation. The SNR measurement is taken from the average of 11 vertically-measured line profiles on the Aluminum step wedge.

#### 4.1.2 Results

The test data are tabulated and summarized in the Appendix. The primary measurement used to analyze the quality of the RADView image is the signal-to-noise ratio (SNR) which is tabulated in the third column of the data sheet along with its measurement

tolerance (+/-). A higher SNR results in a greater ability to detect thickness changes in an object that is on the order of the thickness where the SNR measurement is taken. For this study the measurements are taken between the 1/8" and 3/8" steps of an Aluminum step wedge at 60kV, 60mAs and 60kV, 125mAs.

The square wave response (SWR) is employed to quantify the system's ability to resolve small details in the radiographic signal. For a given noise level, a higher SWR at given line pair resolution (typically 2 line pairs) will result in a greater ability to detect small defects. In the data sheet, the SWR amplitudes for each line pair group on the resolution pattern up to 5.0 line pairs are tabulated.

The noise Wiener spectra show level of noise in the image as a function of line pair frequency. These are shown under the heading "Noise" for discrete line pair frequencies from 0.5 to 4.5 lp/mm.

### **Screen Data Comparisons**

A binder ratio (that is, the weight ratio of binder to phosphor powder) comparison can be made between screens 2060 (or 2061), 2204-02, 2204-04, and 2204-06 for ratios of 4.5%, 10%, 12%, and 15%, respectively. The data indicates that the SNR increases as the binder ratio is decreased; except for the 60kV, 125mAs case, where the 10% binder ratio appears best. In the 60mAs exposure set, this ratio does not appear better than the standard 4.5% ratio. The effect of the binder ratio on the SWR is not so clear. In the 60mAs case, the SWR improves with a higher binder ratio; for the 125mAs exposures, this is not the case. The Noise Wiener spectra indicate that the higher binder ratio results in a higher noise level. This trend is evident in both exposure sets.

Thickness comparison data appears at the bottom of the data sheet. Using screens that consist of the standard phosphor, binder ratio, and screen printed coating method, a thickness variation test was performed. Screens varying in thickness from 4 mils to 13

mils were exposed to the 60k, 60mAs exposure. The data shows that the SNR increases as the phosphor layer thickness is increased. This appears to be a result of a decreased noise level for thicker phosphor layers. For this test - 60kV, 60mAs - the highest SNR occurs on screen 2159-05, the 8 mil screen. The data also shows that the SWR decreases as the phosphor layer increases. The trend ends with the 8 mil thick screen.

The thicker screens, 2187-07 and 2173-10, show slightly abnormal characteristics. The 10 mil screen, 2187-07, appears to have a higher noise level and higher SWR than the trend would predict. Screen 2173-10 did not fit properly through the scanner rollers and frequency miss-fed during testing. Subsequently, this screen has a significantly higher noise level than all of the other screens used in this comparison.

An experimental screen, R&D 101, was manufactured with a 1 mil thick phosphor layer. This screen exhibited a high SWR - approximately 34% at 2 line pairs - and a low SNR. Though manufactured with a different phosphor batch than the other thickness test screens, it confirms the direct relationship between SNR and phosphor layer thickness.

Coating comparison data showing the performance differences between the screen printed coating and the nylon coating were taken. Two pairs of screens were used for a comparison of these coating methods. Screens 2204-02 and 2204-03 are 10% binder ratio screens with standard phosphor that vary only in coating. 2204-02 underwent the standard screen print coating process and 2204-03 is coated with the Nylon coating. The SNR of the screen print coated screen is 60.5 and the nylon coated screen is 53.36. The nylon coated screen however has a significantly higher SWR above 2 lp/mm (34% VERSUS 28% at 2lp/mm). Looking closer at the noise power spectra plots (not included herein), the data shows more low frequency noise for the nylon-coated screens than the screen printed screens. At resolutions above 1 lp/mm, both screens show identical noise levels. These results indicate that the Nylon-coated screens would have a better ability to show fine detail, but in general have slightly lower contrast sensitivity.

The other pair of screens, SMI and 97671001 are manufactured with "No Barium" phosphor and coated by screen printing and Nylon coating, respectively. For these screens, the same higher SWR for the nylon screen is observed as above, except that the two screens have nearly identical in SNR.

The most significant metallurgical change was the removal of Ba from the SrS:Ce,Sm alloy. Ba had previously been added to improve the alloy formation between SrS and the Ce and Sm. However, there was some indication that its removal might increase overall phosphor material efficiency. Screen 9701-42, which contains no Ba, can be compared with standard screens (either 2060 or 2061). The SNR of 9701-42 at 60mAs exposure is 86.2. The SNRs of the standard screens at this exposure are approximately 65. For the longer exposure, 125mAs, 9701-42 has an SNR of 89.9 compared to 75 for the standard screens. In both cases the SWR is 4% higher for the phosphor without the Ba and the noise level is nearly half that of the standard screens. Of all the screens tested, 2219-02 had the highest SNR and did not contain Ba.

Several screens from a different phosphor batch were added to the test pool a few months after initial testing began. The screens were fabricated employing newly installed screen casting equipment under improve temperature and humidity control. These screens, 97042425, SMI, and 97671001, show overall better performance, no matter what the configuration (binder ratio, no barium, coating, etc.), indicating better process control and consistency.

One other area of concern is "flare." Flare measurements are shown in column five of the data spreadsheet. There appears to be a direct relationship between flare and SNR. A higher SNR results in higher flare, confirming the belief that phosphor output and flare are related. For the majority of screens, the phosphor density difference caused by flare is 0.3 (the range of density changes is 0.41 to 0.72).

#### 4.1.3 CONCLUSION

The following conclusions can be drawn from this study:

- SNR increases as the binder ratio is decreased. A lower binder ratio results in lower noise levels, while the SWR remains nearly constant.
- Test results imply that longer exposure may improve the performance of high binder ratio screens.
- Increasing the phosphor layer thickness will increase the SNR - through a decrease in noise level - and decrease the SWR of a phosphor screen.
- A standard composition phosphor layer thickness of 8 mils appears to be optimal for the 60kVx-ray energy used here. This thickness may vary when the Ba is removed.
- Coating the screens with the Nylon improves the SWR almost 35% - i.e., the ability to reproduce small details is greatly improved - but lowers the SNR . The SNR reduction is less significant for the phosphor without Ba.
- Using a phosphor that does not contain Ba improves the SNR approximately 30% for the 60mAs exposure and 20% for the 125mAs exposure.
- Screens with higher SNR have a higher flare measurement.

Based on these results, screens employing no Barium phosphor, nylon coating, and a phosphor layer thickness greater than 4 mils show the optimum performance and will be implemented in production. Overall, roughly a 5-fold increase in screen performance has resulted from the efforts of this program.

## 4.2 Scanner Improvements

### 4.2.1 Light Collector

A key source of noise degrading image quality was found to be a phenomenon referred to as flare. Flare is caused by stray infrared energy illuminating the phosphor screen and generating PSL in an area other than that being directly interrogated by the laser beam. This PSL is added to that produced from the area (pixel) of interest thereby creating an inaccurate density. On the image this appears as a broad horizontal streak from areas of low density to areas of high density. Since approximately 80% of the incident infrared energy is reflected at the surface of the phosphor, there is considerable opportunity for the generation of flare. Several approaches were investigated to reduce this stray infrared. These included narrowing the light collector opening to reduce the amount of phosphor that is exposed to any stray infrared, optimizing coatings in the light collector to absorb stray infrared, and treating the highly reflective stainless steel guide plate behind the phosphor screen (this plate is exposed at either side of the screen as it passes through the scanner) to eliminate back reflection.

Several different slit widths were evaluated showing that as the slit width increased, overall signal increased, as did flare. Conversely, narrowing the slit width reduced the signal as well as the amount of flare. Measurements showed that the optimum compromise between loss of PSL signal versus minimization of flare could be achieved with a slit width of 0.25". Narrower slit widths were found to reduce the PSL signal too much, while making laser alignment extremely difficult. Laser misalignment resulted in highly non-uniform image capture and the presence of vertical artifacts if the laser spot grazed the slit. With the 0.25" width, it was found that laser alignment was more reliable and less prone to variation over time.

In addition to the slit width, the light collector itself was modified relative to the one employed in the 7" scanner. The light collector is a cylinder internally coated with

BaSO<sub>4</sub>, which is a highly reflective material. This results in multiple light “bounces” which help the light captured by the collector to be propagated to the PMT where it can be converted to an electrical signal and digitized. Since the BaSO<sub>4</sub> equally reflects both the visible luminescence from the phosphor, as desired, and the IR, which is undesirable, a selective coating was needed. It was found that Y<sub>2</sub>O<sub>3</sub> can selectively absorb near-IR wavelengths with little absorption of the phosphor’s luminescence. Therefore, a layer of Y<sub>2</sub>O<sub>3</sub> was also applying over the BaSO<sub>4</sub> inside the light collector. Various coating thicknesses were evaluated and the optimum thickness was chosen where the IR absorption of 50% was achieved while maintaining phosphor luminescence reflectance above 80%. With these values, it was possible to reduce IR re-illumination to well below 1% by achieving at least 15 bounces within the collector. In order to aid this, the diameter of the collector was also increased to 6” from the previous 4” diameter. Though the actual efficiency of the light collector is difficult to measure directly, the changes to the light collector design were able to produce 2% sensitivity.

Additional design modifications were also made to prevent any stray IR from re-illuminating the phosphor. One of the key benefits of the present system is that it can accommodate various sizes (widths) of phosphor screens. However, the laser beam always scans a 14” width even if a narrower screen is placed into the reader. Therefore, IR on either of the screen edges can reflect off of surfaces to re-illuminated the phosphor, degrading image quality. Therefore, all surfaces behind the phosphor were also coated to ensure no measurable IR was reflected.

#### **4.2.2 Laser Power and Photomultiplier Tube (PMT) Voltage**

An improvement in image quality, or signal to noise ratio, is obtained by either increasing the number of photons emitted from the phosphor (PSL) for a given exposure, or increasing the number of electrons trapped (longer exposure). The first can be achieved by increasing the laser power used to release the trapped electrons which constitute the latent image. Since only about 10% of the latent image is currently extracted, an increase



in laser power will increase the amount of latent image that is converted to a viewable image. This, therefore, will increase the signal to noise ratio.

Longer exposures can be achieved by adjusting the PMT voltage. Since the PMT voltage is essentially a gain control, the same amount of PSL is emitted from the phosphor screen regardless of the PMT setting. Therefore, while an increase or decrease in PMT voltage increases or decreases the image density, it does not actually improve image quality. What is desired, therefore, is a decrease in PMT voltage that would, in turn, require an increase in exposure to obtain the desired density and improved image quality.

In effect then, adjusting the PMT voltage can be used to produce an effect somewhat analogous to differing speeds of conventional film. That is, a higher PMT voltage will result in a shorter exposure with lower image quality, and a lower PMT voltage will result in a longer exposure with higher image quality. As a result of these studies, the laser power was increased to the maximum and the ability to modify the PMT voltage was added to the system.

It was found that the a maximum laser power of approximately 100 mW at 980 nm could be achieved, though the laser could also become unstable at its highest setting. In order to maintain laser stability, a design containing a chiller was employed in the final system. It was found that laser intensity could be kept constant over long periods and that laser mode hopping was eliminated. This was critical in achieving a 50 micron spot size and uniform scans across a wide area.

#### **4.2.3 Analog-to-Digital (ADC) Converter Slope**

The characteristic curve of the standard system, while providing considerable latitude over conventional film, is quite shallow. Increasing the slope of this curve would, potentially, significantly increase contrast sensitivity. This increase in slope can be accomplished either through image processing or by modifying the slope of the ADC. In

keeping with the philosophy of displaying images that represent raw data, it was decided to take the approach of increasing the ADC slope. This effort demonstrated the feasibility of improving contrast sensitivity. However, further work required to effect a significant improvement would involve a major redesign of the data acquisition circuit board which was beyond the scope of the project.

#### **4.2.4 Transport System**

A key component of the present system was a complete re-design of the transport system required to accurately move a 14" wide screen over a 17" travel path with at least a 70 micron translation pitch. Since the scanning of phosphor screens changes the properties of the phosphor material dynamically, a number of artifacts can be encountered. For example, if the screen transport is not smooth, horizontal banding artifacts (alternating regions of light and dark) can occur which degrade image quality (though absolute sensitivity is unaffected). Similarly, if the plane of the phosphor relative to the beam focus varies during transport, horizontal banding can also occur. Finally, since the screen is transported between two pinch rollers, any misalignments will cause banding at the points where the screen enters or leaves the pinch rollers.

The optimization of the transport mechanism evolved from the initial basic design. The problems encountered with the initial design include severe horizontal banding with roughly a ten-pixel pitch and gross banding at about 1" from the top and bottom of the scan. The small pitch banding was found to be due to poor backing support of the screen during transport. This resulted in the phosphor screen going in and out of the lasers focal plane. The problem was significantly improved, but not fully eliminated, by reducing the gap between the two guide plates between which the screen was transported. The problem with this approach is that reducing the gap also increases the friction on the screen, which leads to a less than smooth screen movement, while increasing the likelihood of damage to the screen.

Two further design changes which will be implemented into commercial units include a spring loaded back plate which ensures a tight gap without overloading the pressure on the screens. Additionally, the pulley ratios have been modified to allow the transport motor to operate at a faster rotational speed where it is more stable. These changes have reduced the fine banding to un-measurable levels. The banding due to the roller transitions was also reduced by tightening the dimensional specifications to ensure proper alignment of the screen being guided into the rollers.

#### 4.2.5 Readout Optics and Resolution

In order to achieve a 50 micron laser spot size over a 14" scan width, additional optical elements were required as compared to the previous 7" scan width. This required design and manufacture of an f-theta lens, as described in the Technical Proposal. The lens was designed and fabricated on schedule and performed as required. The laser beam spot size was measured with the lens, showing a minimum spot size of 45 microns and a +5/-0 spread in size from edge to edge across the 14" width.

One limitation of the present scanner design is that even though a nominally 50 micron spot can be achieved across the 14" width, the data handling electronics cannot presently handle the data that would be generated, which at 50 microns over 14"x17" is over 120 Mbytes. The system is presently limited to a 50 micron pixel pitch up to a 10" width and 70 microns beyond that. This is purely a memory limitation in the acquisition electronics; it is anticipated that the memory limitation will be increased in a future redesign of the acquisition board. With the present design the scan times achieved are as follows:

	<u>100 <math>\mu</math>m</u>	<u>70 <math>\mu</math>m</u>	<u>50 <math>\mu</math>m</u>
7"x10"	56 sec	78 sec	106 sec
7"x17"	90 sec	129 sec	176 sec
14"x17"	92 sec	130 sec	- - -

Additional tests performed indicate that the system exhibits uniform linearity over the 14" width to within 2%. Also, an edge detection algorithm was developed to allow the system to recognize any size screen and to only scan from the screen area. This significantly reduces the amount of useless data that might otherwise be generated.

### **4.3 Image Processing**

A key factor in radiographic examination is still the human inspector viewing an image. More and more, these images are becoming digital because of the benefits of long term lossless storage. Not only is traditional film being quantized, but newer phosphor screen systems provide integral digitization. An important consequence of this trend is the possibility of image enhancement.

Image processing includes both enhancement and restoration, the latter being a method of counteracting degradation based on a knowledge of the mechanism that produced the effect. It is assumed that the typical user of digital systems does not know the physical model causing the deterioration in the image, and so the discussion will be limited to the useful set of tools known as signal enhancement.

Signal enhancement offers sharper contrast, and improved visibility of edges, lines, details and other features. While no information is added in the process, enhancement makes the information more easily viewed, more understandable. Furthermore, enhancement can be specified and controlled and thus offers an objective means for improving an image. Several processes will now be described.

#### **4.3.1 Contrast Enhancement**

Radiographic contrast is defined as the fractional difference in photon fluence between two contiguous regions:  $C = \Delta\Phi / \Phi_0$ , where  $C$  = contrast,  $\Delta\Phi$  = difference in photon fluence, and  $\Phi_0$  = reference photon fluence.

The exposed film or phosphor screen is scanned and digitized. Depending on the characteristics of the scanner-PMT combination, the digital image value emerging from the ADC may have a different contrast than the radiographic contrast. A lookup table (LUT) then makes the final transformation of the digital values into display intensity.

The radiographic contrast is determined by the attenuation coefficient of the material for the incident radiation. And the scanner/PMT/ADC parameters are established to yield generally the best performance, but are limited in adjustability. The display contrast, on the other hand, is determined by the digital LUT table and is the easiest to adjust.

Adjusting the LUT can provide almost arbitrarily high contrast over a selected range of pixel values, while pixels out of that range lose contrast. The function that maps the pixel values to a display intensity is known as the characteristic or gamma function. The dotted line in Figure 5 shows a piecewise-linear characteristic function that provides high contrast to pixels in the range of 0.38 to 0.62. Any pixel with a value greater than 0.62 in this example will have brightness one and any pixel with a value less than 0.38 will have brightness zero. In other words, there is no contrast for pixels outside the selected range.

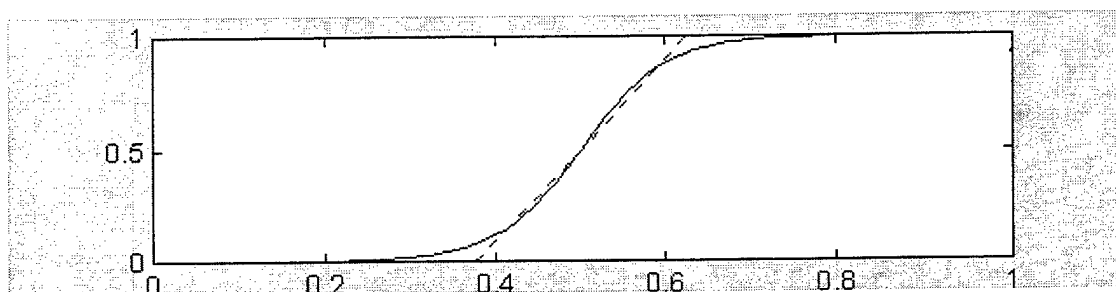


Figure 5. Logistic (solid) overlaid on window/level characteristic curve (dotted).

The solid line shows that a non-linear characteristic curve can produce an arbitrarily high contrast in the region of interest, yet roll off gently enough to provide reasonable contrast at other densities. A simple example is the logistic function  $y = \frac{4}{1 + e^{-2b(x-m)}}$

in which the slope is maximum at  $x = m$ , where  $m$  is the digital input value at maximum contrast. Other than  $m$ , there is only one parameter,  $b$ ; symmetry is retained. Other non-linear functions can be used as well.

### 3.3.2 Histogram Equalization

The purpose of histogram equalization is to redistribute, or map, digital image values so all gray scale intervals will contain an equal number of pixels. At first glance this seems trivial. One can imagine ordering the pixels by gray scale, then assigning them to the available bins in an equitable manner. However, there is a catch. Since indistinguishable levels must be combined, like gray values cannot be separated into different bins. If like gray levels were separated, this would add considerably to the noise, without any real improvement in the signal. Thus histograms usually end up far from having a uniform distribution. Figure 6 illustrates detail enhancement in a pipe elbow and its shroud resulting from histogram equalization.

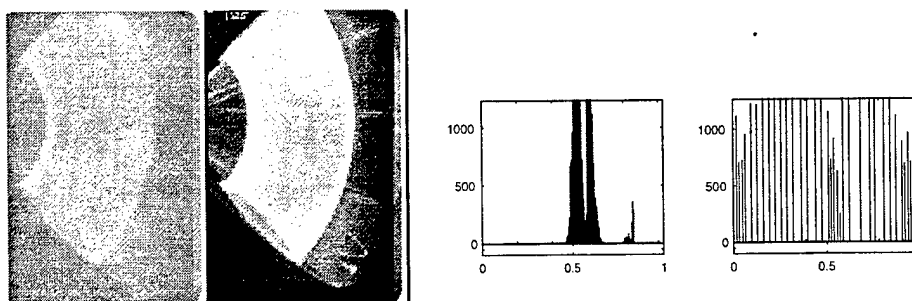


Figure 6. An original image and its histogram before (left) and after (right) histogram equalization.

### 4.3.3 Sharpness Enhancement

The purpose of contrast enhancement discussed earlier is to improve the contrast between two adjacent areas by artificially increasing the (gray level) distance between them. There is a totally different approach which attempts to make the boundary between the regions more conspicuous. It is called unsharp masking. The concept is shown below for a function of a one dimensional variable.

Instead of making extensive alterations in the digital levels of adjacent regions, as in contrast enhancement, unsharp masking emphasizes their boundary. In this way the borders are made more visible. In concept unsharp masking is accomplished by subtracting a low pass filtered version of a signal from itself.

$$I_{enhanced} = I_{original} + \tau \bullet (I_{original} - I_{low\ pass})$$

This results in a new signal or image that overshoots at each transition from one level to another. Unsharp masking can be implemented in this manner. However, there is a better way that squeezes that little bit of extra sharpness from the image, Figure 7.

Subtracting the low frequency content from an image is equivalent to convolving with a high pass filter. When this high pass portion is added back to the original signal, transitions are emphasized. Unfortunately, so is high frequency noise. In order to simultaneously limit the noise and enhance the transition signal, it is best to use a bandpass filter. A excellent function for this application is the Laplacian of Gaussian LoG. This has both the favorable properties of wavelets (of which it is the real part of the Mexican hat wavelet), and a history of successful use as an edge detector. The result of convolution of the LoG with the image is added back to the image (or subtracted, if treating the LoG as a negative quantity).

$$I_{enhanced} = I_{original} + \tau \bullet (\log^* * I_{original})$$

where

$$LoG(x, y) = \frac{-1}{\pi\sigma^4} \left( 1 - \frac{x^2 + y^2}{2\sigma^2} \right) \exp \left[ \frac{-(x^2 + y^2)}{2\sigma^2} \right]$$

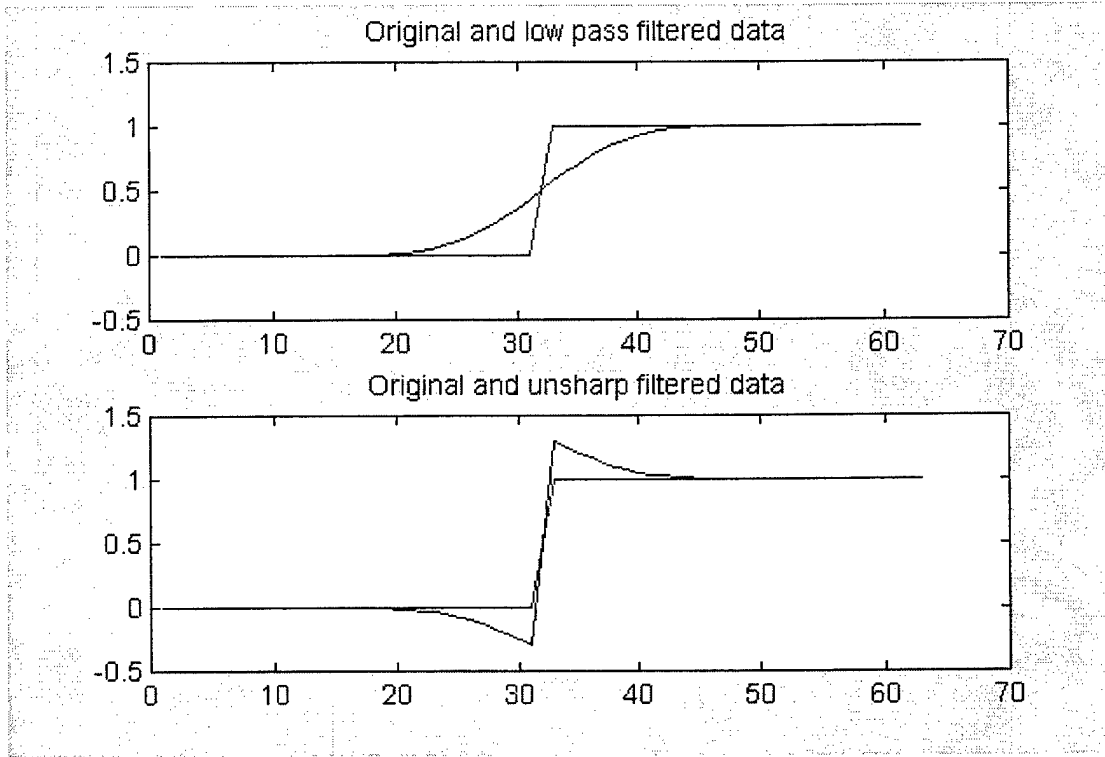


Figure 7. Step function before and after low pass filtering (top), and before and after unsharp mask processing (bottom).

The contribution ( $\tau$ ) and spread ( $\sigma$ ) parameters can be varied to produce slightly different effects. The following two images (unprocessed and unsharp masked resolution pattern) show the improvement possible with LoG enhancement. Our experience is that the LoG works slightly but noticeably better than regular unsharp methods.

#### 4.3.4 Statistical Detail Control

There is an approach in image processing analogous to automatic gain control in electronics. If the signal is too low, the gain is increased. If too high, it is decreased. This



approach has the effect in images to "flatten" the appearance so minor changes appear as important as major changes. However, if there is a lot of detail in the image, the noise may increase. Despite this, the details are emphasized and fine changes made more visible.

As an example, consider the small blade shown in Figure 8. It has many internal ducts which are emphasized by the treatment (although noise is also).

How does this work? It is accomplished by a method called statistical differencing, pioneered by Wallis. Conceptually the differencing is expressed by:

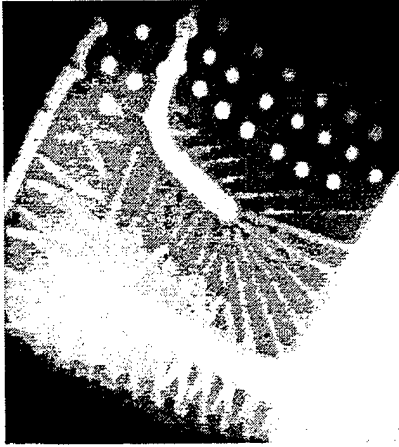
$$I_{ideal} = \frac{I_{actual} - m_l}{s_l} + m_l$$

where

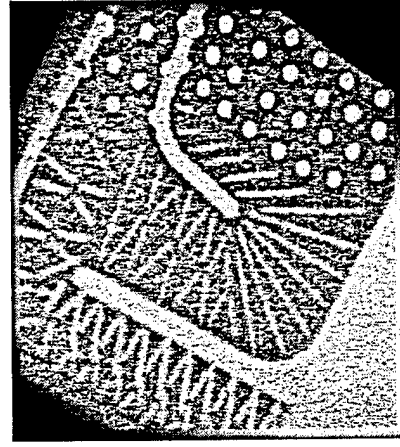
$m_l$  = the local mean value of pixel intensity

$s_l$  = local standard deviation of intensities

The image is allowed to significantly deviate from the local mean only when the local standard deviation is insignificant. When the local variance is high, it is assumed that the deviation of the image from the mean is due to noise.



(a)



(b)

Figure 8. Turbine blade (a) before and (b) after statistical differencing.

Actual implementation can use the following equation:

$$I_{ideal} = \frac{A(I_{actual} - m_l)s_d}{As_l + s_d} + [rm_d + (1-r)m_l]$$

where

A = factor that prevents overly large variation when the standard deviation is small

$m_d$  = desired global mean value

$s_d$  = desired global standard deviation

$r$  = parameter determining relative influence of local versus desired global mean

#### 4.3.6 Crack Detection

Being direction sensitive, this method works best on straight lines. Figure 9 shows an aluminum strut in which a crack can be seen with no special processing, but the crack trails off and it is not clear if it propagates completely from one fastener hole to its

neighbor. Use of a Kirsch edge detector emphasizes features with the directionality of the visible crack and clearly shows that the crack does indeed propagate to the next hole.

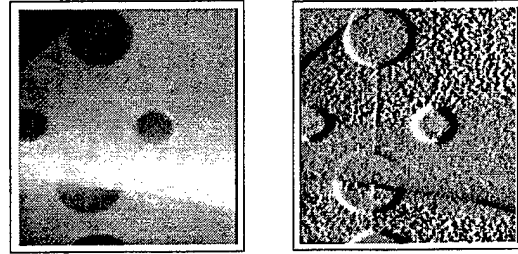


Figure 9. Example of Kirsch filter.

The Kirsch is an example of an edge or gradient detector. For north-south cracks, the gradient direction should be east-west as shown in the following convolution kernel:

$$E = \begin{bmatrix} 5 & -3 & -3 \\ 5 & 0 & -3 \\ 5 & -3 & -3 \end{bmatrix}$$

For other directions the matrix coefficients are rotated accordingly. The various directions can be combined to produce one gradient operator sensitive in all directions by using the maximum response to represent each pixel.

#### 4.3.6 Image Processing Conclusions

While not adding information to an image, enhancement does present the information in a form more visible to the human investigator. Edge sharpening, contrast enhancement, statistical differencing and other techniques were explained and illustrated to show their utility in non-destructive evaluation. Image enhancement is one of the benefits of working in the digital domain. However, it must be emphasized that while processing is advantageous, "raw" data must be preserved. In addition, any processing techniques

employed become an integral part of documented technique, similar to source-to-film, energy, and exposure time.

## **5.0 DEVELOPMENT OF 14" SCREENS**

### **5.1 Scale-up of Screen Fabrication Process**

#### **5.1.1 Company-funded facility improvements**

Once the phosphor chemistry and screen design were chosen, the phosphor lab had to be upgraded to be able to manufacture the 14" screens reliably. The first major improvement was the installation of an air conditioning system. The phosphor powder and phosphor slurries are extremely sensitive to humidity. The phosphor powder cannot be manufactured in an area that does not have a controlled environment. The current laboratory facilities did not contain adequate environmental controls. An air conditioning system was installed to control the heat and humidity during the summer months so that production could continue even when the weather turns hot and humid. Two dehumidifiers were also installed with the air conditioning.

Another major improvement was the installation of a clean room facility. During the tape casting of the phosphor slurries, the cast tapes have to dry before they can be moved. During this drying process, dust and dirt from the environment can fall onto the drying tapes marring the surfaces and contaminating the effects of the phosphor. After the installation of the clean room, the production yield, and consistency, of the screens increased greatly.

Equipment had to be purchased to accommodate the larger production screens. A larger casting table and casting blade were purchased to make the larger screens. Larger curing ovens and storage cabinets were also purchased.

### 5.1.2 Environmental and flexibility testing

When the screens were fabricated, they were tested for environmental effect of heat, humidity, and thermal cycling and compared against the former production screens. For these tests, an environmental chamber was rented so that controlled heat and humidity tests could be conducted.

The first test performed was on the protective packaging. Four screens were placed in the chamber at 95°F and 95% humidity. One was exposed, one was in a cassette, one was in a fold over anti-static bag, and one was in a 4 mil thick zip lock bag. Four of the previous production screens were also tested under the same condition. Both of the exposed screens were yellowed after 24 hours but the screen sustained less damage than the production screen. The screen cassette and the anti-static bag offered minimal protection, but the zip lock bag protected both screens from damage.

A hot mandrel test was performed on both screen types. The screens were placed into a cassette and wrapped around a 2" mandrel. They were placed into the environmental chamber and the temperature was raised to 120°F for 30 minutes. Both screen types survived without damage.

A thermal shock test was performed on both types of screens. The screens were placed inside cassettes and wrapped around a 2" mandrel. Over a 24 hour period, the screens were subjected to thermal cycling going from -40°F to 120°F with no humidity. Both screens survived. When the test was repeated with humidity being introduced during the heating part of the cycle, the screens yellowed at the point where they were bent around the mandrel.

The conclusions of these tests indicated that the screens are very sensitive to humidity. The Mantech screens offer slightly more protection than the previous production screens, but for storage in high humidity environments (>50% RH), additional protection is still

needed to prevent screen damage, such as zip lock plastic bags. The screens can survive severe temperature cycling, even bent around a 2" mandrel, however, if there is humidity present, damage could still occur.

## **5.2 Reusability Testing (Subcontract to Southwest Research Institute)**

To characterize the effect of reuse of the phosphor screen, Liberty contracted Southwest Research Institute (SwRI) to perform an evaluation of the reusability of the phosphor screen. The intent of the test was to evaluate the screens for any possible degradation in the phosphor's ability to generate a latent image, convert the latent image to a viewable image, or return to an erased state after reuse of the screen approximately 500 times. In essence, to see if there was any change in the solid state process after repeated use. The concept was to x-ray a test phantom, read and store the image, erase the image, and then do the same test over and over. The images would be analyzed for signs of phosphor degradation.

### **5.2.1 Technical Approach**

SwRI designed and fabricated a test phantom which consisted of the following:

- A 0.25" steel bar that extends over one complete edge of the phantom.
- An aluminum step wedge ranging in thickness from 0.125" to 1.0" in increments of 0.125".
- Two line-resolution test fixtures - one with horizontal lines and one with vertical lines; the lines are copper wires with diameters of 0.002", 0.003", 0.004", 0.005", and 0.008".
- A 0.25" aluminum plate with 2T and 8T penetrameters.
- A 0.5" aluminum plate with 2T and 10T penetrameters.

These items were epoxied onto a 0.06" plexiglass plate and placed in a frame, which allowed the cassette to be reloaded in the same position repeatedly.

Algorithms were developed for monitoring the image quality. The size of the images stored by the RADView system was approximately 34 megabytes, which was too large for the Matlab data processing software. Therefore, a C program was written that extracted smaller regions of the images and stored them as 16-bit binary data files with no headers. These smaller regions, then, could be read into Matlab for processing.

Resolution was measured from the line test fixtures. A full width at half max measurement was taken, as well as a contrast measurement from both the horizontal and vertical test wires. Background noise and contrast degradation were quantified by statistical measures on the step wedge and the steel bar. The statistical measures used were mean, standard deviation, skew, and kurtosis. Skew and kurtosis are statistics based on the third and fourth central moments of the sampled data. Skew gives a measure of the symmetry of the distribution of samples. Kurtosis is a measure of the peakedness of the distribution relative to a normal (Gaussian) distribution.

All test exposures were shot at 60 kV for 120 mAs and erasure of the phosphor screen consisted of 5 minutes under sodium/IR light followed by 5 minutes under IR light.

### **5.2.2 Discussion**

Five hundred twenty exposures were accomplished over the testing period and, based upon the data obtained, no trend of image degradation was observed. Between two and three exposure/read/erase cycles were accomplished per hour. Occasionally, less than this number of cycles was accomplished because the normal 5 minute erasure proved to be inadequate, so an additional erasure cycle was needed. Erasure times of 6 minutes or more produced significantly better results. It should be noted that the eraser used in these tests was not the improved one developed under this project. Use of the delivered system



by the 4<sup>th</sup> Fighter Wing at Seymour Johnson AFB, NC has demonstrated an effective eraser time of 3 minutes.

Early in the testing it was noted that when the phosphor screen was read after exposure, vertical lines would appear in the image. However, these lines would never appear in the exposed x-ray image. It is believed that these lines were a type of mechanical mark made by the scanner. The scanner used in these tests was an early 7" wide version. Modifications made to the transport system for development of the 14" wide scanner for this program eliminated this artifact.

Data analysis was performed on the images obtained from 520 exposures. These measurements were taken on eight regions of each exposure file. These regions included each of the four penetrameters, the horizontal and vertical resolution wires, the step wedge, and the 0.5" thick steel block. Statistical measurements were made (approximately) on every tenth exposure from the resolution wires, the step wedge, and the 0.5" steel block.

Statistics measured from the wires were contrast and full-width-at-half-maximum (FWHM) value. The contrast was defined as the brightness difference between the peak of a wire and the average of several background pixels near the wire. The FWHM was defined as the width of the wire signal at the point where the signal reaches  $\frac{1}{2}$  of its maximum value. The FWHM measurement was made with subpixel resolution by linear extrapolation.

Neither the FWHM nor the contrast measurements of all five vertical and horizontal wires showed any significant degradation trend over the 520 exposures of the phosphor. It should be noted that a pixel size of 50 microns (0.002") was used and that all five wires of 0.002", 0.003", 0.004", 0.005", and 0.008" diameters were visible and measurable.

The mean, standard deviation, skew and kurtosis were measured for each individual step of the step wedge. No degradation trend was observed over the 520 exposures. Consistently, the density across each step fell off drastically before the edge of the step. This was due to flare resulting from the configuration of the laser, collector tube, and other elements of the older 7" scanner used for these tests. This effect was corrected in the redesign for the 14" wide scanner in this project. This flare effect was consistent throughout the test and did not interfere with observing possible degradation trends.

For the 0.125" aluminum plate, the penetrameters used were the .12 ASTM and the .62 MIL-STD-453. All three holes in the ASTM penetrameter were detected and none of the holes in the MIL-STD penetrameter were detected. For the 0.25" aluminum plate, .25 and 1.2 MIL-STD-453 penetrameters were used. All three holes were visible in the 1.2 penetrameter, and the 2T and 4T holes were visible in the .25 penetrameter. It should be noted that the purpose of this test was to assess degradation over time, not resolution and hence, the technique was not optimized to detect particular penetrameter holes.

The mean density value and standard deviation measurements on the steel bar did not show any significant trend over the 520 exposures. Except for occasional spikes due to erroneous data, the skew and kurtosis remained approximately constant for all exposures.

In conclusion, the phosphor screens were subjected to 520 exposure/scan/erase cycles. Based on the data obtained, no trend of image degradation was observed. The data included:

1. The peak contrast values as a function of exposure obtained from the line fixture with five vertical wires.
2. The FWHM values as a function of exposure measured from the line fixture with five vertical wires.

3. The peak contrast values as a function of exposure obtained from the line fixture with five horizontal wires.
4. The FWHM values as a function of exposure measured from the line fixture with five horizontal wires.
5. The mean pixel value of the various steps in the step wedge as a function of exposure.
6. The pixel standard deviation from the mean value for steps 1 through 7 in the step wedge as function of exposure.
7. The skew as a function of exposure for each of the eight steps of the wedge.
8. The kurtosis for each of the steps of the wedge.
9. The average pixel value in a region over the 0.5" thick steel bar.
10. The skew values for the steel bar image.
11. The kurtosis values for the steel bar image.

## **6.0 DEVELOPMENT OF 14" CASSETTES**

Development of cassettes to accept the 14" screens was a straightforward scale-up of the existing cassettes. The same paper for the envelope itself (the same as that used for some radiographic film cassettes) and the same closure mechanism of velcro-attached magnetic bars that interface to the scanner opening were used.

## **7.0 ERASER DEVELOPMENT**

The eraser development program had two major goals. The first was to determine the optimal erasing wavelengths and power level; the second major goal was to create an eraser design that could accommodate a 14"x17" phosphor screen.

### **7.1 Erase process optimization**

The existing 7" eraser was a dual light source unit, that is, it employed a low pressure sodium (SOX) lamp producing 590 nm wavelength yellow light followed by a halogen lamp filtered to pass 825+ nm wavelength (IR) light. The technique employed was to bathe the exposed phosphor screen in the SOX light first for about 5 minutes then illuminate the screen with the IR light for about 5 minutes. This dual source process produced erasure levels down to about 1.0 phosphor density.

In an attempt to improve upon the original system eraser, an extensive test program was conducted to examine the erase process and techniques employed. The first step was to quantify the effectiveness of various light wavelengths for erasure. This was accomplished by illuminating an exposed phosphor screen using a white light source through a variety of optical filters. It was quickly determined that the yellow/orange/red and near infrared wavelengths all provided some degree of erasure. Refinement of the experiment revealed that a long pass filter, which passed 710nm and longer, erased screens more completely than other wavelengths.

Once the erasure wavelength was determined, an engineering prototype eraser was designed and fabricated. This test bed permitted easy change out of light sources, rapid modification of lamp to screen distance and it also was used to refine the control circuitry. A variety of lamp types were tested to determine beam spread angles and uniformity of cast light. The adjustable filter stage permitted easy testing of aperture sizes, configurations, and positioning within the light path, all of which were done to optimize the uniformity of the light cast upon the screen holding tray. From this prototype testing came the final design points such as lamp type, lamp to screen distance, lamp position, filter aperture shape and size and the control circuit scheme.

The test program showed that erasure speed and final erase level was a function of the incident power on the screen. The old eraser design used a single 150W halogen bulb to produce the infrared wavelengths but it had an incidence angle of only about 15 degrees. The new design eraser incorporates six 75 Watt MR16 bulbs at a 90 degree incidence. The bulbs have a very uniform 36 degree beam spread coupled with aluminum reflectors that project almost all energy toward the screens. With this configuration, it was found that a fully saturated screen could be erased to below a 1.0 digital phosphor density after scanning within 5 minutes. It was not possible to reduce erase times any more than this. This suggests that the trapping population is quite high and that a large time is required to remove the residual trapped electrons. It is believed that further improvements in erase time will likely have to come about by modifications to the phosphor material composition.

## **7.2 Sheet metal Design**

Many improvements were made to the erase design to improve system throughput, reduce damage to the phosphor screens and to enhance system manufacturability. Eraser throughput was enhanced by designing the pullout screen tray to simultaneously accommodate up to four 7"x10" screens, two 7"x17" screens or one 14"x17" screen. The previous eraser design could only accommodate two 7x10 screens simultaneously or one

7x17 screen. Light baffling was added around the pullout tray to permit daylight operation of the eraser. The addition of a semi-automated control system, which incorporated an adjustable timer and an automatic shutoff, improved the usability of the unit.

The design was also altered so screens would be placed phosphor side up, thereby facing the erasing light source through air. The old eraser design utilized a glass tray upon which the charged phosphor screens were placed. This could cause accumulation of dirt on the screens as well as potential for scratching or heat damage. The erasing tray design also allows a user to easily pickup a phosphor screen; this could be difficult when using the older glass tray design. Design for manufacturability & maintainability was another goal of this work effort. The light bar module, which contained the lamps and step down transformer, and the timer control module were both designed as subassemblies which could be built and tested as independent units. These could then be integrated into a final finished eraser at a later time. This modular design permits a service technician to rapidly troubleshoot and replace a failed module.

## 8.0 APPLICATIONS RESULTS

One of the key requirements of this program was demonstration of 2-2T sensitivity on aluminum. Figure 10 shows digital images obtained with the prototype system employing optimized screens. The images show 2%-2T to 2%-1T sensitivity for the indicated thicknesses. Figure 11 shows a line pair gauge scanned at 70 micron resolution, indicating a limiting resolution of 7 Lp/mm, as expected.

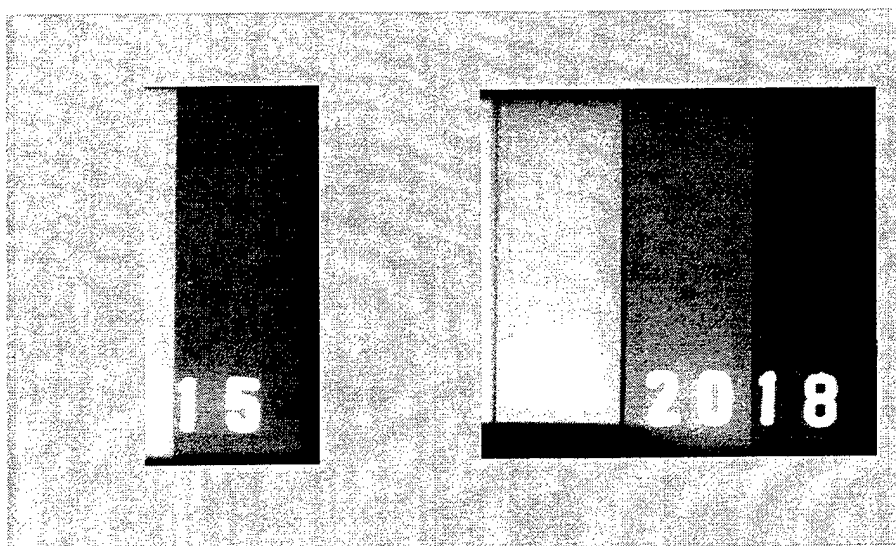


Figure 10. 2% ASTM penetrameters on aluminum step wedge.

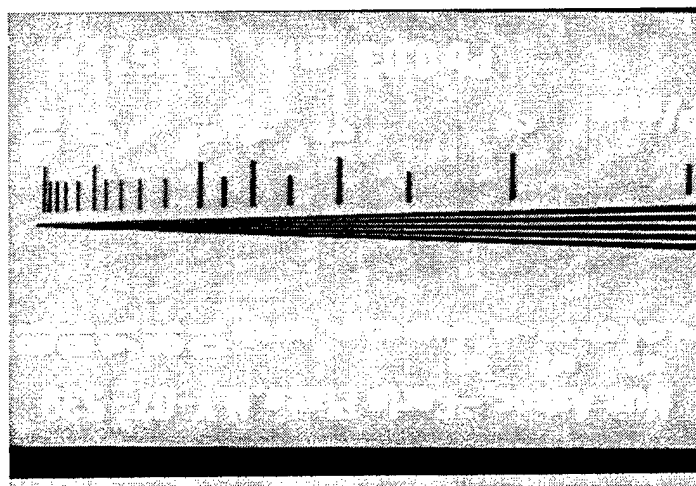


Figure 11. Lead resolution pattern exposed and scanned at 70 microns, showing 7 Lp/mm resolution.

Figure 12 shows a full 14"x17" scan of composites, aluminum blocks and a lead resolution pattern. The image was scanned at 70 micron resolution. Figure 13 shows a Ni orbital tube weld, demonstrating required image quality.

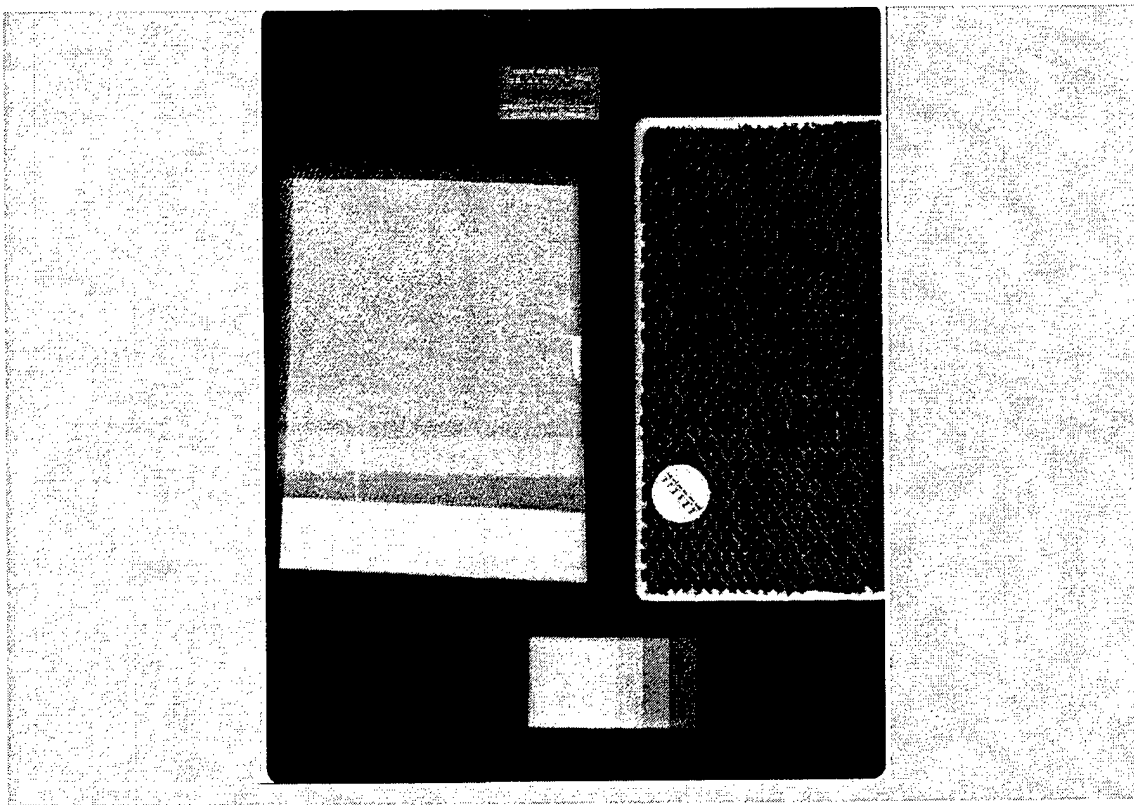


Figure 12. Full 14"x17" image of composite phantom of object, aluminum blocks, and line pair gauge.

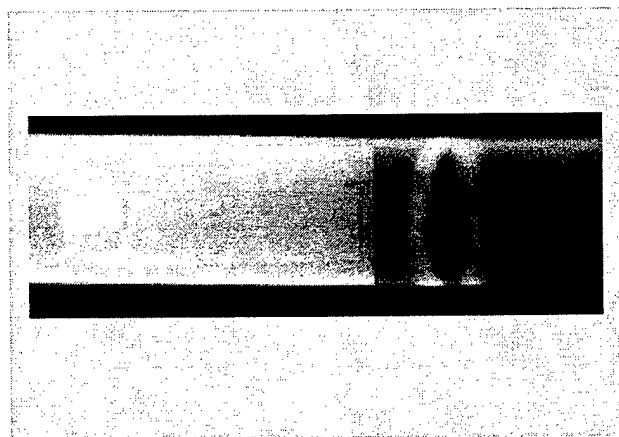


Figure 13. X-ray image of Ni orbital tube weld, approximately 19 mm in diameter.



## 9.0 CONCLUSIONS

This effort successfully demonstrated its key objectives:

1. Demonstration of 2%-2T contrast sensitivity
2. Increasing imaging field of view to 14"x17" area
3. Installation of three units at USAF sites for field use

The results have also demonstrated that adequate reliability and durability can be achieved at both the system level and with the media. The environmental and reusability studies do show that the phosphor screens are still susceptible to moisture induced degradation, but most phosphor materials exhibit some level of moisture sensitivity. By employing basic care, it should be reasonable to achieve approximately 1000 uses per screen in a harsh field environment; reusability will be greater if the screens are employed in a clean and dry environment. It should also be noted that the cost basis for the screens should be based on usability, meaning that the important parameter is cost per shot relative to film. For example, a \$500 screen that lasts 1000 exposures is \$0.50/exposure, or about 1/10<sup>th</sup> the cost of raw film alone. We have also found that the cost basis for the screen is volume driven, meaning that as the volume goes up, cost and price come down reducing the need for unreasonably high reusability rates. It is not realistic to expect phosphor screens of any type would last much beyond 1000 exposures in a field environment.

Since the completion of the initial phase of this program, the systems have been further fine-tuned and were commercially released in early 1998. A derivative product, which is designed for use with an alternate storage phosphor material having different optical readout characteristics, has also been developed. This system has been developed by Lumisys and targeted successfully to the medical radiology market and can scan the type of phosphor material manufactured by Agfa and Kodak. A modified version of this system has also been introduced by Liberty for NDT use employing Agfa storage

phosphor screens. During the last three quarters of 1998, Liberty installed six such CR systems covering both aerospace and other NDT applications. Continued improvements and development of the derivative product for the much higher volume medical market have also helped reduce system costs to well below \$100,000, making the systems much more affordable and accessible to a broader range of the NDT market.

### **Current Status of USAF Units**

The systems have changed location from the original installation sites. The Warner Robins system is now located at Wright Patterson AFB, Seymore Johnson's system is at Edwards AFB and Kelly's is located at Tinker AFB.

The system that is at Wright Patterson is in the NDE Research Lab. However, a number of items were not shipped from Warner Robins to Wright Patterson. We are awaiting identification of the missing or lost items in order to bring the systems up to proper working order.

Tinker has completed their evaluation of the system and submitted a report to Wright Patterson. Tinker has mostly metallic x-ray inspection looking for fatigue cracks. Their x-ray application requires special cut film in moon, finger, and other non-standard dimensions. They thought the image quality was adequate, and believe that this is one of the futures for x-ray. However, they appear to need the ability to cut the phosphor screens to the shapes needed for their applications. This is one of the benefits of our current system, and Tinker should be made aware of the systems flexibility to handle different sizes and shapes.

Edwards AFB has the third system. After the system was received, several items came up missing, such as cables and their document scanner. These items had been replaced but the software in the system seems to have been corrupted. The systems have since been reformatted by Liberty and upgraded to the most current version of software. On

06/22/99, Liberty personnel set up the system at Edwards, verified system functionally, setup a data base, and radiographed an F 15 honey comb wing section. The expected image quality was obtained and additional basic instruction was given to the NDE staff to operate the system. The primary concern at Edwards was the amount of time it takes to erase a screen and the number of screens they would have to buy in order to keep the same production schedule when they get an aircraft in for inspection. This suggests that an automated erasing station may be needed to support high volume applications.

## 10.0 RECOMMENDATIONS

The program has clearly achieved its goals of scaling up and improving the performance of a storage phosphor filmless radiography system for aircraft inspection. The next step in this process is to identify specific applications and develop detailed procedures for using the system. It has been found that the field sites are extremely busy with production work and unless there is a specific procedure approved for use on a particular application, they can do little more than perform system evaluation when time permits. Therefore, a systematic approach is required to methodically replace film x-ray inspection applications with filmless radiography.

A second issue is that the workstations and software currently in the field employ hardware that was state-of-the-art 3 years ago when the systems were developed, but are now obsolete. Not only has computing hardware improved in performance during this period of time, but Liberty has continued to release new versions of its software. Finally, as was already mentioned, a derivative product designed to read barium fluorohalide chemistry storage phosphors produced by Agfa, Kodak, and Fuji has also been developed. There are certain advantages and disadvantages of this system, which are also worth exploring from an applications and usability standpoint.

In summary, the recommendations for future work are as follows:

1. Determine how best to implement the storage phosphor systems in production.
2. Upgrade the three units to current hardware and software levels.
3. Investigate the use of new readout systems employing barium fluorohalide phosphors, particularly for higher energy applications.

## 11.0 REFERENCES

"The Advanced Development of X-Ray Computed Tomography Applications," WL-TR-93-4016 Boeing Defense and Space Group.

"Reusability Testing of the Liberty Phosphor Screen," Final Report SwRI Project 17-8808, NDE Science and Technology Division, Southwest Research Institute, San Antonio, TX.

Marr, D. and E. Hildreth. "Theory of edge detection," *Proc. Royal Society*, London, B 207, pp.187-217, 1980.

Gonzalez, Rafael C. and Paul Wintz. *Digital Image Processing* (second edition). Reading, Mass.: Addison-Wesley, 1987.

Pratt, William K. *Digital Image Processing* (2nd Edition). NY: Wiley, 1991.

Lee, Chongmok, David O. Wipf, Allen J. Bard, Keith Bartels and Alan C. Bovik, "Scanning electrochemical microscopy. 11. Improvement of image resolution by digital processing techniques," *Analytic Chemistry*, vol. 63, no. 21, pp. 2442-1447, November 1, 1991.

## **Appendix I**

### **Economic Considerations**

(from Technical Proposal)

Liberty Technologies, Inc. developed a system of digital radiography that was specifically geared to be cost-effective to the industrial market. It was priced in such a way (\$100,000 to \$150,000 for a maximum 7"x17" phosphor image, and depending on options) as to provide a return on investment (ROI) of one to two years depending on the operating environment. The amount of x-ray film used in the Air Force has been estimated at \$1M per year. This cost does not include the cost of film processors, film processing chemicals, or silver recovery units necessary to recover environmentally hazardous byproducts of the film development process. In addition, significant man-hours are expended to continuously maintain and manage film processing and archiving.

Discussions with, and visits to, several Air Force organizations reveal a wide variety of operating scenarios. However, some generalizations can be made and conclusions drawn from them. The F-15 requires the highest level of radiography. F-15s receive a phase inspection every 200 flight hours. Every 200 hours the vertical and horizontal stabilizers, flaps and ailerons are inspected. Every 400 flight hours inspection of the ramp ribs, closure ribs, wing spars, and ramps are added to the 200 hr. phase inspection. Every 1200 flight hours inspection of the wing tips, horizontal stabilizer tips, inboard/outboard ramps, speed brake and rudder are added to the 200 hr. and 400 hr. inspections.

According to the 1<sup>st</sup> FW at Langley AFB, an F-15 fighter wing with approximately 72 aircraft will, on the average, perform about 9 phase inspections per month and spend approximately \$3,600 for chemicals in one year. The actual number of 200, 400, and 1200 hour inspections will vary from place to place depending on the age distribution of aircraft. For example, a unit with older aircraft will perform more 1200 hour inspections, while a unit with newer aircraft will perform more 200 and 400 hour inspections. If one assumes that, on average, more 200 hour inspections will be performed than 1200 hour

inspections, etc., we can estimate that in one month a "typical" wing will perform 6 each 200 hour inspections, 2 each 400 hour inspections, and 1 each 1200 hour inspection. These inspections would cost the following (estimates on number of pieces of film per inspection, and price per piece of film come from the 1<sup>st</sup> FW):

200 hour inspection = 116 pieces of film

400 hour inspection = 318 pieces of film

1200 hour inspection = 336 pieces of film

6 ea. 200 hour, 696 film @ \$4.50 ea. = \$3,132

2 ea. 400 hour, 636 \$2,862

1 ea. 1200 hour, 336 \$1,512

9 1668 film \$7,506 x 12 months = \$90,072

+ \$3600=\$93,672/yr

Discussions were also held with the 46<sup>th</sup> FW at Eglin AFB, FL. Of all the radiography inspections in the F-15's NDI manual, they identified which ones are performed at each of the 200 h, 400 h, and 1200 h phase inspections. These are included in the Table below, T.O. 1F-15A-36 RT Inspection Summary. A 400 hour inspection will include those inspections indicated as 400 h as well as those indicated as 200 h inspection. Also, a 1200 h inspection will include all those indicated as 200 h, 400 h, and 1200 h inspections.

Table. T.O. 1F-15A-36 RT Inspection Summary

Part/Assembly	Page	Defect/Conditon	# Exp.	# Film	Size	Film Type	Phase
Torque Box Main Spar	2-61	Fatigue Cracks	2	2	7x17	AA or M	N/A
Wing Tip Assy.	2-96	Water Entrapment	4	11	14x17	D7	200
Wing Tip Assy.	2-99	Foam Adhesive Separation	11	13	7x17	D7	200
Wing Tip Closure Rib	2-108	Fatigue Cracks	9	9	7x17	D7	400
Wing Tip Fwd. Spar	2-112	Fatigue Cracks	1	2	7x17	AA/M	N/A
Flap Assy.	2-115	Water Entrapment	5	15	14x17	D7	200
Flap Assy.	2-118	Foam Adhesive Separation	20	20	7x17	D7	200
Aileron Assy.	2-131	Water Entrapment	3	12	14x17	D7	200
Aileron Assy.	2-134	Foam Adhesive Separation	14	14	7x17	D7	200
Intermediate and Main Spars	2-162	Distortion or Breaks	3	3	14x17	M	400
Outbd. T.E. Ribs	2-168	Fatigue Cracks	4	4	7x17	AA	400
			1	1	14x17	AA	
Outbd. Torque Box Ribs	2-182	Fatigue Cracks	3	12	7x17	AA/M	400
			1	2	7x17	AA/M	
Stabilator Outbd. L.E. Box	3-5	Water Ent/Foam Adh. Sep.	5	9	14x17	D7	200
Stabilator Torque Box	3-24	Water Entrapment	3	13	14x17	AA	200
Stabilator Torque Box	3-28	Foam Adhesive Separation	26	26	7x17	AA	200
Stabilator Aft Box	3-51	Water Entrapment	4	19	14x17	D7	200
Stabilator Aft Box	3-54	Foam Adhesive Separation	14	17	7x17	D7	200
Stabilator Tip	3-67	Water Ent/Foam Adh. Sep.	1	3	14x17	D7	1200
Rudder	3-92	Water Ent/Foam Adh. Sep.	4	9	14x17	D4	1200
			1	2	14x17	D4/D7	
Var. Inlet Ramp, Inbd. Panel	4-32	Water Entrapment	1	2	14x17	AA/M	1200
Var. Inlet Ramp, Rib Support	4-35	Cracks	2	4	14x17	M	400
Var. Inlet Ramp, Inbd. Panel	4-44	Skin to Core Bond	2	4	14x17	D7	1200
Var. Inlet Ramp, Outbd. Panel	4-49	Water Entrapment	3	3	14x17	D7	1200
Var. Inlet Ramp Assy.	4-52	FOD	12	25	14x17	AA	400
			2	8	14x17	AA/M	
No.1 Var. Inlet Ramp Assy.	4-55	FOD	4	7	14x17	AA	N/A
			4	10	7x17	AA	
Var. Inlet Ramp, Outbd Panel	4-62	Skin to Core Bond	1	1	14x17	D7	1200
Var. Inlet Ramp, Outbd Panel	4-70	Skin to Core Bond	1	1	14x17	D7	1200
Composite Speed Brake	4-78	Cracks in Adhesive	8	16	7x17	D7/D4	1200
Composite Speed Brake	4-82	Water Entrapment	28	28	14x17	AA	1200



			4	4	7x17	AA	
Vertical Stab., Fwd. Box	4-137	Water Entrapment	4	13	14x17	D7	20C
Vertical Stab. Torque Box	4-153	Water / Closure Cracks	1	2	14x17	AA	20C
Vertical Stab. Torque Box	4-156	Foam Adhesive Separation	28	28	7x17	AA	20C
Vertical Stab. Aft Lwr. Box	4-174	Water Entrapment	1	5	14x17	D7	20C
Vertical Stab. Aft Lwr. Box	4-177	Foam Adhesive Separation	1	1	7x17	D4	20C
			4	4	7x17	D7	
Fairing Assy.	4-201	Water / Foam Adh. Sep.	2	4	14x17	D7/D4	N/A
			252	388			

35 Total RT Inspections (23 film are double loaded, 113 are multiple films exposed simultaneously ,  
and 184 are 7x17, and 204 are 14x17)

Note: These figures should be doubled for the entire aircraft)

If it is again assumed that a 72 aircraft wing will perform about 9 phase inspections a month, and the number of film for each of those inspections is calculated from T.O. 1F-15A-36:

200 hour inspection = 396 pieces of film

400 hour inspection = 532 pieces of film

1200 hour inspection = 678 pieces of film

6 ea. 200 hour, 2376 film @ \$4.50 ea. = \$10,692

2 ea. 400 hour, 1064 \$ 4,788

1 ea. 1200 hour, 678 \$ 3,051

9 4118 film \$18,531x 12 months = \$222,372

+ \$3600 = \$225,972/yr

It is believed that the estimate from the 1<sup>st</sup> FW is low, while the estimate calculated directly from the NDI manual is unrealistically high. Nevertheless, if a median number of \$150,000 per year is used for film and maintenance costs, then a "typical" F-15 wing will pay for a RADView system in a year's time. While these numbers are estimates, it is clear that there is a distinct near-term economic benefit associated with transitioning from film to digital radiography technology.

# Appendix II Phosphor Optimization Data

Experiment No.		Description	SWR												
			Lp/mm												
			SNR	+/-	Flare	0.05	2.00	2.24	2.50	2.80	3.15	3.55	4.00	4.50	5.00
60kV, 60mAs															
2060		(Standard)	63.29	3.4	0.508	1.000	0.295	0.246	0.215	0.153	0.119	0.089	0.068	0.047	0
2061		(Standard)	67.88	2.8	0.584	1.000	0.275	0.214	0.152	0.141	0.104	0.068	0.051	0.040	0.029
2204-02		(10% binder)	60.53	2.5	0.493	1.000	0.281	0.228	0.184	0.145	0.109	0.075	0.055	0.037	0
2204-04		(12% binder)	52.88	1.3	0.498	1.000	0.294	0.235	0.185	0.147	0.111	0.078	0.057	0.039	0
2204-06		(15% binder)	51.01	2.1	0.415	1.000	0.308	0.251	0.203	0.160	0.121	0.083	0.061	0.043	0
9701-42		(Nylon,no Ba)	86.24	1.6	0.644	1.000	0.343	0.284	0.238	0.188	0.144	0.104	0.075	0.052	0
2204-03		(Nylon)	53.36	1.2	0.515	1.000	0.341	0.279	0.228	0.182	0.140	0.100	0.072	0.048	0
2219-02		(No Barium)	91.84	2.1	0.721	1.000	0.270	0.220	0.180	0.137	0.102	0.071	0.052	0	0
R&D101		(Thin Cast)	24.74	0.7	0.251	1.000	0.335	0.282	0.236	0.191	0.151	0.115	0	0.065	0
R&D103		(B250 NoBa)	39.95	1.2	0.729	1.000	0.267	0.222	0.185	0.146	0.112	0.082	0.061	0.046	0
R&D105		(B250 STD)	64.31	1.9	0.458	1.000	0.280	0.233	0.193	0.153	0.118	0.085	0.063	0.046	0
SMI		(Sterling binder)	57.36	0.7	1.026	1.000	0.262	0.212	0.175	0.137	0.105	0.075	0.056	0.041	0
97042425		Standard	73.98	1.7	0.601	1.000	0.264	0.209	0.164	0.132	0.101	0.069	0.048	0.033	0
97671001		(Sterling/Nylon)	56.56	1.9	0.977	1.000	0.346	0.293	0.256	0.192	0.148	0.103	0.077	0.061	0.036

<u>60kv,125mAs</u>		<u>SNR</u>	<u>+/-</u>	<u>Flare</u>	<u>0.05</u>	<u>2.00</u>	<u>2.24</u>	<u>2.50</u>	<u>2.80</u>	<u>3.15</u>	<u>3.55</u>	<u>4.00</u>	<u>4.50</u>	<u>5.00</u>
2060	(Standard)	76.50	2.3		1.000	0.296	0.244	0.198	0.157	0.117	0.083	0.060	0.043	0
2061	(Standard)	74.49	2.4		1.000	0.280	0.229	0.189	0.146	0.110	0.078	0.056	0.041	0
2204-02	(10% binder)	83.57	2.1		1.000	0.269	0.215	0.178	0.132	0.101	0.074	0.056	0.033	0.033
2204-04	(12% binder)	66.92	1.3		1.000	0.257	0.206	0.166	0.129	0.096	0.067	0.048	0.033	0
2204-06	(15% binder)	64.23	1.4		1.000	0.272	0.224	0.197	0.141	0.105	0.070	0.051	0.030	0.031
9701-42	(Nylon,no Ba)	89.92	2.1		1.000	0.345	0.281	0.217	0.187	0.145	0.108	0.078	0.059	0
2204-03	(Nylon)	73.21	1.9		1.000	0.314	0.258	0.216	0.167	0.128	0.090	0.066	0.047	0
2219-02	(No Barium)	112.05	3.5		1.000	0.269	0.216	0.175	0.137	0.103	0.072	0.052	0.036	0
R&D101	(Thin Cast)	29.44	1.2		1.000	0.344	0.293	0.239	0.200	0.158	0.118	0.089	0.065	0
R&D103	(B250 NoBa)	52.86	1.3		1.000	0.285	0.234	0.194	0.155	0.119	0.086	0.064	0.045	0
R&D105	(B250 STD)	98.47	2.9		1.000	0.254	0.216	0.186	0.142	0.107	0.074	0.057	0.044	0.037
SMI	(Sterling binder)	76.94	3.4		1.000	0.259	0.209	0.172	0.134	0.102	0.072	0.053	0.038	0
97042425	Standard	95.72	1.8		1.000	0.273	0.226	0.181	0.140	0.104	0.072	0.053	0.036	0
97671001	(Sterling/Nylon)	70.77	1.6		1.000	0.339	0.283	0.238	0.187	0.143	0.105	0.074	0.051	0

<u>Noise</u>		<u>Ip/mm</u>	<u>0.5</u>	<u>1.0</u>	<u>1.5</u>	<u>2.0</u>	<u>2.5</u>	<u>3.0</u>	<u>3.5</u>	<u>4.0</u>	<u>4.5</u>
2060	(Standard)		7.55E-04	6.45E-04	4.71E-04	3.31E-04	2.77E-04	2.17E-04	1.99E-04	1.45E-04	1.34E-04
2061	(Standard)		6.52E-04	5.58E-04	3.72E-04	3.21E-04	2.30E-04	2.05E-04	1.73E-04	1.31E-04	1.26E-04
2204-02	(10% binder)		5.33E-04	4.32E-04	2.90E-04	2.20E-04	2.09E-04	1.63E-04	1.34E-04	1.26E-04	1.27E-04
2204-04	(12% binder)		4.97E-04	4.60E-04	2.91E-04	2.67E-04	2.23E-04	1.76E-04	1.26E-04	1.14E-04	1.35E-04
2204-06	(15% binder)		6.51E-04	5.92E-04	4.28E-04	2.88E-04	2.32E-04	1.98E-04	1.63E-04	1.28E-04	1.32E-04
9701-42	(Nylon,no Ba)		3.74E-04	2.96E-04	2.35E-04	2.07E-04	1.64E-04	1.30E-04	1.17E-04	9.60E-05	8.58E-05

2204-03	(Nylon)	5.88E-04	4.95E-04	3.54E-04	2.94E-04	2.41E-04	1.76E-04	1.68E-04	1.37E-04	1.29E-04
2219-02	(No Barium)	4.83E-04	3.82E-04	2.76E-04	2.72E-04	1.63E-04	1.60E-04	1.12E-04	9.92E-05	9.34E-05
R&D101	(Thin Cast)	1.16E-03	1.14E-03	8.82E-04	6.14E-04	5.79E-04	4.28E-04	3.62E-04	3.05E-04	2.64E-04
R&D103	(B250 NoBa)	6.54E-04	4.77E-04	3.50E-04	2.85E-04	2.63E-04	1.97E-04	1.71E-04	1.49E-04	1.33E-04
R&D105	(B250 STD)	5.26E-04	4.13E-04	3.27E-04	2.74E-04	2.17E-04	1.93E-04	1.48E-04	1.33E-04	1.14E-04
SMI	(Sterling binder)	6.47E-04	4.59E-04	3.66E-04	2.52E-04	2.27E-04	1.82E-04	1.46E-04	1.57E-04	1.32E-04
97042425	Standard	3.81E-04	2.98E-04	2.47E-04	1.95E-04	1.75E-04	1.47E-04	1.26E-04	1.14E-04	9.94E-05
97671001	(Sterling/Nylon)	6.59E-04	4.82E-04	3.85E-04	3.55E-04	2.48E-04	2.15E-04	1.66E-04	1.56E-04	1.38E-04

60kV,125mAs

		<u>0.5</u>	<u>1.0</u>	<u>1.5</u>	<u>2.0</u>	<u>2.5</u>	<u>3.0</u>	<u>3.5</u>	<u>4.0</u>	<u>4.5</u>
2060	(Standard)	8.13E-04	6.04E-04	4.36E-04	3.01E-04	2.41E-04	1.91E-04	1.47E-04	1.50E-04	1.18E-04
2061	(Standard)	7.14E-04	5.02E-04	4.31E-04	3.03E-04	2.20E-04	2.20E-04	1.46E-04	1.20E-04	1.07E-04
2204-02	(10% binder)	4.97E-04	4.21E-04	2.97E-04	2.59E-04	1.75E-04	1.40E-04	1.25E-04	9.95E-05	9.63E-05
2204-04	(12% binder)	5.86E-04	4.32E-04	2.99E-04	2.57E-04	1.87E-04	1.51E-04	1.16E-04	1.16E-04	1.23E-04
2204-06	(15% binder)	6.68E-04	5.51E-04	3.98E-04	2.99E-04	2.23E-04	1.78E-04	1.52E-04	1.24E-04	1.09E-04
9701-42	(Nylon,no Ba)	4.40E-04	3.48E-04	2.77E-04	1.97E-04	1.56E-04	1.33E-04	1.00E-04	8.78E-05	7.74E-05
2204-03	(Nylon)	5.43E-04	4.51E-04	3.65E-04	2.56E-04	2.21E-04	1.68E-04	1.53E-04	1.33E-04	1.07E-04
2219-02	(No Barium)	4.64E-04	3.55E-04	2.82E-04	2.33E-04	1.67E-04	1.45E-04	1.08E-04	9.71E-05	8.91E-05
R&D101	(Thin Cast)	1.56E-03	1.39E-03	1.06E-03	8.86E-04	6.38E-04	4.79E-04	3.57E-04	3.33E-04	2.67E-04
R&D103	(B250 NoBa)	6.83E-04	4.98E-04	3.96E-04	2.99E-04	2.35E-04	1.96E-04	1.75E-04	1.64E-04	1.39E-04
R&D105	(B250 STD)	5.08E-04	3.55E-04	3.26E-04	2.87E-04	2.00E-04	1.66E-04	1.28E-04	1.18E-04	1.00E-04
SMI	(Sterling binder)	5.66E-04	3.87E-04	3.70E-04	2.47E-04	2.20E-04	2.03E-04	1.53E-04	1.25E-04	1.19E-04
97042425	Standard	3.34E-04	2.56E-04	2.39E-04	1.52E-04	1.36E-04	1.27E-04	9.34E-05	8.92E-05	8.10E-05
97671001	(Sterling/Nylon)	7.46E-04	5.68E-04	4.69E-04	3.26E-04	2.71E-04	2.26E-04	2.09E-04	1.49E-04	1.48E-04

# Thickness Comparison

<u>SWR</u>	<u>SNR</u>	<u>+/-</u>	<u>Flare</u>	<u>0.05</u>	<u>2.00</u>	<u>2.24</u>	<u>2.50</u>	<u>2.80</u>	<u>3.15</u>	<u>3.55</u>	<u>4.00</u>	<u>4.50</u>
2060	(4-4.5 mil)	60.37	2.0	1.49	1.000	0.321	0.262	0.214	0.169	0.128	0.061	0.042
2061	(4-4.5 mil)	66.92	1.0	1.54	1.000	0.283	0.231	0.188	0.147	0.111	0.053	0.036
2160-06	(6 mil)	68.39	2.2	1.65	1.000	0.262	0.210	0.170	0.127	0.093	0.043	0.030
2159-05	(8 mil)	78.20	1.5	1.6	1.000	0.237	0.185	0.146	0.111	0.080	0.038	0.026
2187-07	(10 mil)	74.58	1.9	1.47	1.000	0.252	0.200	0.161	0.121	0.089	0.045	0.029
2173-10	(13 mil)	75.62	1.5	1.73	1.000	0.229	0.179	0.139	0.103	0.072	0.034	0.023
<u>Noise at 1/8" AI (Vertical)</u>												
2060	(Standard)	8.77E-04	6.66E-04	6.89E-04	5.58E-04	5.20E-04	5.32E-04	5.27E-04	4.58E-04	4.16E-04		
2061	(Standard)	8.44E-04	6.65E-04	6.64E-04	6.02E-04	5.34E-04	5.26E-04	5.37E-04	4.94E-04	4.80E-04		
2160-06	(6 mil)	7.19E-04	6.93E-04	5.82E-04	5.68E-04	5.58E-04	5.29E-04	4.39E-04	5.20E-04	4.64E-04		
2159-05	(8 mil)	5.05E-04	4.90E-04	4.76E-04	4.13E-04	4.09E-04	3.92E-04	4.06E-04	4.26E-04	3.78E-04		
2187-07	(10 mil)	5.76E-04	4.96E-04	4.62E-04	4.54E-04	4.23E-04	5.68E-04	3.76E-04	4.33E-04	4.17E-04		
2173-10	(13 mil)	1.35E-03	8.25E-04	5.68E-04	5.80E-04	4.29E-04	3.96E-04	4.04E-04	3.85E-04	3.61E-04		